Nonintegrable Schrödinger discrete breathers

J. Gómez-Gardeñes[a] and L. M. Floría
Departamento de Teoría y Simulación de Sistemas Complejos, Instituto de Ciencia de Materiales de Aragón, C.S.I.C.-Universidad de Zaragoza, 50009 Zaragoza, Spain and Departamento de Física de la Materia Condensada e Instituto de Biocomputación y Física de los Sistemas Complejos (BIFI), Universidad de Zaragoza, 50009 Zaragoza, Spain

M. Peyrard
Laboratoire de Physique, Ecole Normale Supérieure de Lyon, 69364 Lyon, France

A. R. Bishop
Theoretical Division and Center for Nonlinear Studies, Los Alamos National Laboratory, Los Alamos, New Mexico 87545

(Received 5 June 2004; accepted 10 September 2004; published online 22 November 2004)

In an extensive numerical investigation of nonintegrable translational motion of discrete breathers in nonlinear Schrödinger lattices, we have used a regularized Newton algorithm to continue these solutions from the limit of the integrable Ablowitz–Ladik lattice. These solutions are shown to be a superposition of a localized moving core and an excited extended state (background) to which the localized moving pulse is spatially asymptotic. The background is a linear combination of small amplitude nonlinear resonant plane waves and it plays an essential role in the energy balance governing the translational motion of the localized core. Perturbative collective variable theory predictions are critically analyzed in the light of the numerical results. © *2004 American Institute of Physics*. [DOI: 10.1063/1.1811991]

Discrete breathers are spatially localized, time periodic solutions of homogeneous nonlinear lattices, which have been recently observed in experiments on a variety of physical systems (magnetic solids, arrays of Josephson junctions, coupled optical waveguides and photonic crystals). Though many of the properties of discrete breathers are today well characterized, the question on their mobility remains under controversy, due to the radiative losses unavoidably associated to the translational motion of the localized pulse in generic (nonintegrable) systems. We address here this problem in an important class of nonlinear lattices: *the discretizations of the nonlinear Schrödinger equation*. Our results show that exact mobile breather solutions ride over an extended excited state of the lattice, which we fully characterize. Moreover, this background plays an essential role in the energy balance required for exact nonintegrable mobility.

I. INTRODUCTION

Nonlinear lattices have become the subject of a considerable multidisciplinary interest, with applications in physics subdisciplines as diverse as biophysics (myelinated nerve fibers,[1] DNA,[2] biopolymer chains[3]), nonlinear optical devices (photonic crystals[4] and waveguides[5,6]), and Josephson effect[7] (superconducting devices,[8,9] Bose–Einstein condensates[10–12]), among others. From a theoretical perspective they have been progressively recognized not as mere discretizations (unavoidable for numerical computations) of nonlinear continuum field equations, but as a target of interest in their own right, due to the distinctive features associated with *discreteness*, whose relevance to experimental features have been largely established.

More specifically, among the variety of observable nonlinear behaviors of lattice dynamics, the phenomenon of (discrete breathers) nonlinear localization in lattices[13] has received attention in both experimental and theoretical research during the last several years. (Nontopological) discrete breathers are exact spatially localized, time-periodic solutions. Due to discreteness the plane wave spectra are bounded, thus making possible the absence of multiharmonic resonances of the exact discrete breather solution with extended modes. The combination of nonlinearity and discreteness is sufficient for the physical existence of discrete breathers, DBs for short, resulting in its generality and broad interest. The reader may find in Ref. 14 a recent multidisciplinary survey of current research on the subject.

Our primary concern here is the issue of the DBs' mobility. The translational motion of discrete breathers introduces a new time scale (the inverse velocity), so generically a moving breather excites resonances with plane wave band spectra. This fact poses no problem to the persistence of localization when the lattice dynamics is governed by power balance (forced and damped lattices[15]): the emitted power is exactly compensated by the input from the homogeneous external force field, during stationary breather motion. However, for generic (nonintegrable) Hamiltonian lattices, the radiative losses would tend to delocalize energy, and some energy compensating mechanism is needed in order to sustain exact stationary states of breather translational motion. From the (particle) perspective of collective variables theory,

[a]Electronic mail: gardenes@unizar.es

the localized breather experiences a periodic Peierls–Nabarro potential function of its position, so that the motion of the localized field oscillation over this landscape should be expected to induce the emission of radiation at the expense of translational (and/or internal) breather kinetic energy, which thus would unavoidably decay on time.

To address the problem, a reasonable strategy is to use precise numerical techniques on adequately general models, with the hope that they may pave the way to further physical (and mathematical) insights. Our chosen model belongs to an important class of nonlinear lattice models: the discretizations of the continuum nonlinear Schrödinger equation, here referred to as nonlinear Schrödinger (NLS) lattices. First of all, they are ubiquitous in models for polaronic effects in condensed matter, nonlinear optical technologies, and the physics of Bose condensate lattices and superconducting devices, where nonlinear localization is currently studied. Second (a very convenient technical advantage), this class contains an integrable limit (the Ablowitz–Ladik lattice, see below) having exact moving discrete breathers, wherefrom perturbation (collective variable) theories have been developed in support of exact (or very approximate, in the least) nonintegrable mobile DBs. This allows a detailed theoretical analysis of the numerical results, as well as eventual feedbacks for useful (and currently used) theoretical concepts and perspectives. In Sec. I A of this introduction we present the (three-parameter) NLS lattice that we have studied, originally introduced by Salerno.[16]

The numerical techniques employed are summarily introduced in Sec. II. We stress here the unbiased character of this numerical procedure which, unlike other techniques, is not based on ansatze on the expected functional form of the exact solution sought. In essence, the procedure uses a regularized Newton continuation method for operator fixed points, and it only requires a good starting set of parameter values where the exact solution is known. In our case this is provided by the integrable Ablowitz–Ladik limit of the NLS lattice, from which adiabatic continuation of the two-parameter (core frequency ω_b and velocity v_b) family of moving Schrödinger breathers is performed.

The main numerical facts are shown in Sec. III. The numerical solutions are found to be (up to numerical precision) the superposition of a travelling exponentially localized oscillation (the *core*), and an extended background, which is a linear superposition of finite amplitude nonlinear plane waves $A\exp[i(kn-\omega t)]$ (see Fig. 1). The amplitudes of these resonant nonlinear plane waves are observed to differ typically by orders of magnitude, so that only a small number of them are relevant for most practical purposes. They fit well simple theoretical (thermodynamic limit) predictions based on discrete symmetries requirements. Contrary to the exact immobile breather solution (space-homoclinic and time-periodic orbit), which asymptotically connects the rest state (vacuum or ground state) of the lattice with itself, each exact mobile localized solution is instead homoclinic to a specific lattice state of extended radiation. In other words, exact stationary mobility of discrete breathers requires an extended excited state of the lattice. Preliminary accounts of some of the numerical results of this section were reported in Ref. 17.

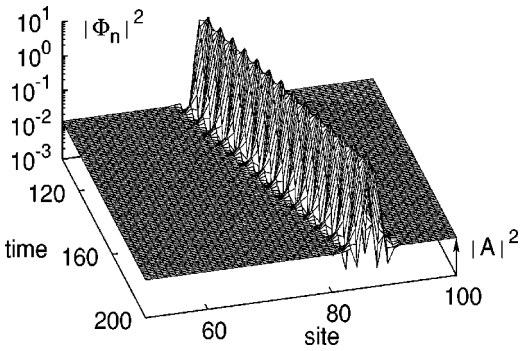

FIG. 1. Time evolution of $|\Phi_n|^2$ profile of a mobile discrete Schrödinger breather. The frequency of the solution is $\omega_b=5.050$ and the velocity is $v_b=0.804$. Note that the background is composed by a single plane wave with amplitude A. The nonintegrable parameter of Eq. (7) is $\nu=0.2$.

In Sec. IV we analyze the numerical results in the light of collective variable theories, correlating them with the main theoretical predictions of this successful (however incomplete) physical perspective. In particular, the existence of Peierls–Nabarro barriers to translational core motion is confirmed, and its subtle relation to the background amplitude is discussed. We present also numerical confirmation of the existence of exact oscillating anchored breathers, whose extended background is much smaller than those of traveling discrete breathers of the same internal frequency ω_b. Along with the discussion in this section, a physical interpretation of the role of the interaction background-core in the energy balance emerges, paving the way to a satisfactory integration of the results into a collective variable theory.

Finally, in Sec. V, after summarizing the main conclusions drawn on discrete Schrödinger breather mobility, we briefly trace some interesting open questions for further research, notably the approach to irrational breather time scales ratios, the study of multibreather solutions (two-breather collision processes, trains of moving breathers), and the coupling to both thermal and nonthermal (e.g., elastic) degrees of freedom, where the numerical tools and results presented here can find further applications.

A. NLS lattices

The standard discrete nonlinear Schrödinger (DNLS) equation[1,18] is the simplest discretization of the one-dimensional continuous Schrödinger equation with cubic nonlinearity in the interaction term, i.e.,

$$i\dot{\Phi}_n = -C(\Phi_{n+1}+\Phi_{n-1}) - \gamma|\Phi_n|^2\Phi_n. \tag{1}$$

In this expression $\Phi_n(t)$ is a complex probability amplitude, the parameter C amounts the nearest neighbor coupling, and γ is the strength of the nonlinearity. The self-focusing effect of local nonlinearity balanced by the opposite effect of the dispersive coupling makes possible the existence of localized periodic solutions (breathers) of the discrete field, where the profile of $|\Phi_n|$ decays exponentially away from the localization center:

$$\Phi_n(t) = |\Phi_n| \exp[i\omega_b(t)]. \tag{2}$$

In the uncoupled limit $C \to 0$ of the DNLS equation, also known as the anti-integrable or anti-continuous limit, discrete breathers can be easily constructed by selecting a periodic oscillation $\Phi_{n_0}(t)$ of frequency ω_b at site n_0 and $\Phi_n = 0$ for $n \neq n_0$. These solutions can be uniquely continued to nonzero values of the coupling C, and constitute the one-parameter family of immobile on-site breathers of the DNLS equation.

Unfortunately the continuation from the uncoupled limit does not provide solutions where the localization center moves along the lattice with velocity v_b, i.e., mobile discrete breathers. On the other hand, there is an integrable lattice as a limit of the nonlinear Schrödinger class that possesses this type of mobile solution. That is the one discovered by Ablowitz and Ladik in Ref. 19:

$$i\dot{\Phi}_n = -C(\Phi_{n+1} + \Phi_{n-1})\left[1 + \frac{\gamma}{2}|\Phi_n|^2\right], \tag{3}$$

where, again, C and γ account for the strength of the coupling and the nonlinearity, respectively. The integrable Ablowitz–Ladik equation, A-L for short, possesses a two-parameter family of exact moving breather solutions of the form

$$\Phi_n(t) = \sqrt{\frac{2}{\gamma}} \sinh\beta \,\mathrm{sech}\,[\beta(n - x_0(t))] \times \exp[i(\alpha(n - x_0(t)) + \Omega(t))]. \tag{4}$$

The two parameters of this breather family can be chosen to be the breather frequency ω_b and velocity v_b,

$$v_b = \dot{x}_0 = \frac{2\sinh\beta \sin\alpha}{\beta}, \tag{5}$$

$$\omega_b = \dot{\Omega} = 2\cosh\beta\cos\alpha + \alpha v_b, \tag{6}$$

where $-\pi \leqslant \alpha \leqslant \pi$ and $0 < \beta < \infty$. The A-L moving breather (instantaneous) profile interpolates between the rest state $\Phi_n = 0$ of the lattice (at $n \to \pm\infty$) in an exponentially localized region around $x_0(t)$, while traveling with velocity v_b.

The connection between the integrable (though physically limited) A-L equation and the physically relevant (though nonintegrable) DNLS equation is provided by the model originally introduced by Salerno in Ref. 16,

$$i\dot{\Phi}_n = -(\Phi_{n+1} + \Phi_{n-1})[C + \mu|\Phi_n|^2] - 2\nu\Phi_n|\Phi_n|^2. \tag{7}$$

This lattice provides a Hamiltonian interpolation between the standard DNLS equation (1), for $\mu = 0$ and $\nu = \gamma/2$, and the integrable A-L lattice when $\mu = \gamma/2$ and $\nu = 0$. The Hamiltonian of the Salerno equation is given by

$$\mathcal{H} = -C\sum_n (\Phi_n\overline{\Phi}_{n+1} + \overline{\Phi}_n\Phi_{n+1}) - 2\frac{\nu}{\mu}\sum_n |\Phi_n|^2 + 2\frac{\nu}{\mu^2}\sum_n \ln(1 + \mu|\Phi_n|^2), \tag{8}$$

which contains the A-L and DNLS Hamiltonian for the above limits. In addition to the Hamiltonian, this equation possesses, for any value of the parameters, the following conserved norm:

$$N = \frac{1}{\mu}\sum_n \ln(1 + \mu|\Phi_n|^2). \tag{9}$$

In the following we will set the value of $\gamma = 2$ (as usual) and consider the coupling strength $C = 1$ in Eq. (7).

The continuation of the family of mobile discrete breathers from the A-L integrable limit allows numerical observations of the interplay between the integrable term, weighted by the parameter μ, and the nonintegrability, weighted by ν.

II. DISCRETE BREATHER NUMERICS

We introduce here the numerical techniques that we have used. As a whole, one could refer to them as the (SVD-) regularized Newton method. They do not constitute a novel method in "discrete breather numerics," as they have been already used, e.g., in Ref. 20, to refine moving breathers of Klein–Gordon lattices obtained by other numerical means (see, by contrast, Ref. 21). From the methodological side, what is novel here is the systematic use of them in the investigation of the family of moving Schrödinger breathers reported in Sec. III.

To some extent, the presentation here is self-contained. First, in Sec. II A we introduce the notion of (p,q) resonant solution, providing some illustrative examples. The (SVD) regularized Newton algorithm is presented in Sec. II B, and finally in Sec. II C we briefly explain the basics of Floquet stability analysis.

A. Discrete space–time symmetries: (p,q) resonant states

If a frequency $\omega_b = 2\pi/T_b$ is given, we will say that a solution $\Phi = \{\Phi_n(t)\}$ is (p,q) *resonant* with respect to the reference frequency ω_b, if the following condition holds, for all n and t:

$$\Phi_n(t) = \Phi_{n+p}(t + qT_b). \tag{10}$$

After q T_b-periods, these solutions repeat the same profile but displaced by p lattice sites. In more technical terms, these (p,q) resonant solutions are fixed points Φ of the operator

$$\mathcal{L}^p\mathcal{T}^q = \mathcal{M}, \tag{11}$$

$$(\mathcal{M} - \mathcal{I})\Phi = 0, \tag{12}$$

where $\mathcal{L}$ and $\mathcal{T}$ are, respectively, the lattice translation and the T_b-time evolution operator:

$$\mathcal{L}\{\Phi_n(t)\} = \{\Phi_{n+1}(t)\}, \tag{13}$$

$$\mathcal{T}\{\Phi_n(t)\} = \{\Phi_n(t + T_b)\}. \tag{14}$$

We now consider some examples of (p,q) resonant solutions with respect to the frequency ω_b; the first example is simply provided by the family of plane wave solutions of Eq. (7):

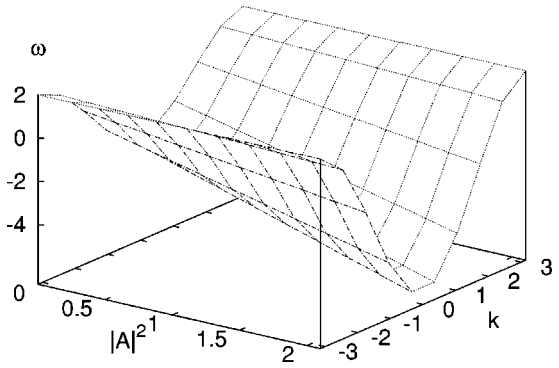

FIG. 2. Plot of the nonlinear dispersion relation surface of nonlinear plane waves, Eq. (16), as a function of the amplitude A and the wave number k of the plane wave. The values of μ and ν are fixed to 0.5.

$$\Phi_n(t) = A \exp\left[i(kn - \omega t)\right]. \tag{15}$$

It is easily seen, by inserting (15) in Eq. (7), that the values of ω, k and $|A|$ define a surface in the three-dimensional space, the nonlinear *dispersion relation surface* $\omega(k,A)$ (see Fig. 2):

$$\omega = -2[1 + \mu|A|^2]\cos k - 2\nu|A|^2. \tag{16}$$

Note that due to the nonlinear character of Eq. (7), the frequency ω depends on both wave number k and amplitude $|A|$ of the plane wave.

One can easily determine those plane waves that are (p,q) resonant with respect to ω_b: Eq. (10) imposes the following condition on ω and k:

$$\frac{\omega}{\omega_b} = \frac{1}{q}\left(\frac{p}{2\pi}k - m\right), \tag{17}$$

where m is any arbitrary integer. These planes in the 3D space $(\omega,|A|,k)$ intersect the dispersion relation surface at (in general) several one-parameter families (branches) $k_j(|A|)$, in the first Brillouin zone $(-\pi \leqslant k \leqslant \pi)$.

If we are not interested in unreasonably large (and not interesting) amplitude values $|A|$ of the plane waves, the number of branches is finite: one can see that for fixed values of all the parameters (p,q,ω_b,ν,μ), there is a finite number of branches in the limit $|A| \to 0$; there is also a well defined (parameter dependent) threshold value of the amplitude at which a pair of new branches (tangent bifurcation) appears (i.e., these plane waves can only resonate with ω_b for amplitudes above some threshold value).

Thus, by a suitable bounding of the amplitude, for each couple (p,q) one finds a finite number, s, of branches of (p,q) resonant plane waves. (Note also that this number diverges when p/q tends to an irrational.)

A different, and highly nontrivial, example of (p,q) resonant solutions is provided by the solitary waves (4) of the A-L lattice. From Eq. (6) it is clear that the choice $2\pi v_b/\omega_b = p/q$ selects a (p,q) resonant solitary wave with respect to the frequency ω_b. The set of velocity values of resonant A-L breathers is dense and any A-L moving breather is a limit of some sequence of resonant ones. Note also that immobile breathers are (0,1) resonant with respect to the frequency ω_b.

In the integrable limit, the plane waves and the A-L breathers are both exact independent solutions. Integrability makes possible that the initial localization of energy is maintained with time evolution, without decaying away by exciting radiation. It is a well established result that (even far away from this integrable limit) immobile discrete breathers remain exact solutions of the lattice dynamics. Our concern in the next sections is the question of moving discrete breathers away from integrability in Eq. (7). In order to study them, we will focus on (p,q) resonant solutions. The motivating of this restriction comes from its accessibility to numerics. First we will motivate the numerical (Newton) method that allows us to study these solutions with an adequately high precision.

B. Newton continuation

A well-known numerical procedure to obtain exact periodic solutions of nonlinear lattices is the Newton continuation.[20,22–24] The different practical implementations of this procedure work very successfully when, for example, one obtains numerically exact immobile discrete breathers of Eq. (7), from the uncoupled limit $\mu=0$ and $C=0$, where exact periodic discrete breathers are trivially constructed.

The iteration of the Newton operator $\mathcal{T}$ converges rapidly to its fixed point (i.e., the solution to be computed) provided the starting point, $\hat{\Phi}^0$, is close enough, and the solution of the following system of linear equations is a well-posed problem:

$$(D\mathcal{T} - 1)(\Phi^n - \Phi^{n+1}) = [\mathcal{T} - \mathcal{I}]\Phi^n, \tag{18}$$

where $D\mathcal{T}$ is the Jacobian matrix of the Newton operator, and Φ^n [the nth iteration solution of (18)] converges quadratically to the fixed point solution. By adiabatic change of a model parameter, one constructs a uniquely continued exact fixed point solution for each parameter value, using each time, as starting point of the Newton iteration, the solution previously computed.

The matrix $(D\mathcal{T}-1)$ must be invertible, in order to uniquely compute Φ^{n+1}. Degeneracies associated with the +1 eigenvalues of $D\mathcal{T}$, if any, have to be removed in order to obtain a unique fixed point solution. When continuing immobile (periodic) discrete breathers of Eq. (7), a convenient prescription is commonly used, namely to restrict the operator action to the subspace of time-reversible solutions.[22,23] This provides a practical way of removing degeneracies, allowing unique continuation of immobile discrete breathers.

For the continuation of (p,q) resonant solutions (of which periodic solutions are only the particular case $p=0$ and $q=1$), one has to use $\mathcal{M} = \mathcal{L}^p\mathcal{T}^q$ as the Newton operator. One has also to deal with the degeneracies of $\mathcal{M}$, and imposing time-reversibility could, in this case, be too restrictive.

A well-known solution to the problem of removing degeneracies when no clear restrictions are available is provided by the so-called *singular value decomposition* (SVD)[20,22,25,26] of the matrix $(D\mathcal{L}^p\mathcal{T}^q - 1)$:

$$(D\mathcal{L}^p\mathcal{T}^q - 1) = J = PVQ, \tag{19}$$

where P, V and Q are $2N\times 2N$ square matrices. P and Q are orthogonal matrices and V is diagonal ($v_j\delta_{ij}$) with possibly null (zero) elements, called singular values, associated with the null space of J (the subspace that is mapped to zero $Jx=0$). The columns of P whose same-numbered elements v_j are nonzero are an orthonormal set of basis vectors that span the range of J (the subspace reached by this matrix). The rows of Q whose same-numbered elements v_j are zero are an orthonormal basis for the null space of J. One can numerically use this SVD decomposition, checking the (numerical) vectors spanning the null space to identify degeneracies, and using at iteration steps the pseudoinverse matrix

$$Q^* \hat{V}^{-1} P^*, \tag{20}$$

where $\hat{V}^{-1}$ is diagonal with elements $1/v_j$ for $v_j \neq 0$ and 0 for $v_j = 0$.

As a judicious test of our numerical codes, we have used both procedures (reduction to time-reversible subspace and SVD decomposition) to obtain immobile discrete breathers of the Salerno model. Both agree, up to the highest possible accuracy, from the uncoupled limit (one- and two-site breathers) up to the A-L limit (and vice versa).

This test serves also to provide further confirmation of an important and well-known theoretical result. At the integrable A-L lattice, one- and two-site immobile breathers are but two particular choices of the continuous one-parameter (x_0, the localization center) family of immobile solitary waves, i.e., constant $x_0(t)=n$ or $n+\frac{1}{2}$, respectively, in Eq. (4). The well-known result, confirmed by our numerics, is that away from the A-L limit *only* these (one- and two-site) immobile discrete breathers persist under adiabatic continuation. No immobile breather centered in between exists. For positive values of the parameter ν, the one-site immobile one has a lower value of energy $\mathcal{H}$, and it is a linearly stable solution, while the energy of the two-site breather is higher and it is linearly unstable. The relative situation is reversed for negative values of ν. This result can be interpreted as the emergence of a (Peierls–Nabarro) potential function of the breather center x_0, which destroys the continuous degeneracy of immobile breathers, leaving only two of them per lattice unit, namely those localized at maxima and minima of the Peierls potential. This interpretation, which is captured in the theoretical framework of collective variable approaches, turns out to play a central role in building up the physical interpretation of the numerical results on mobile discrete Schrödinger breathers, below (Sec. III).

The numerical integration of the equations was performed using a fourth-order Runge–Kutta scheme with time step $T_b/500$. The convergence criterion for the fixed point solution is that the value of $\Sigma_j|([\mathcal{T}-\mathcal{I}]\Phi^{n+1})_j|$ is less than $N\times 10^{-16}$ (where N is the size of the lattice). The typical size of the lattices was taken between 100 and 200 sites depending on the characteristics of the solution considered, as we will explain in Sec. III.

C. Floquet stability analysis

A very useful outcome of the numerical Newton method of computing solutions of Eq. (7) is the Jacobian matrix of the Newton operator, usually called the Floquet matrix F. This matrix is the linear operator associated with the linear stability problem[27] of the fixed point solution.

Indeed, the Jacobian F of the Newton operator $\mathcal{M}$,

$$F = D\mathcal{M}, \tag{21}$$

maps vectors in the tangent space of the solution [small initial perturbations $\vec{\epsilon}(0)$ of the fixed point solution] into their $T_{\mathcal{M}}$-evolved vectors, i.e., $\vec{\epsilon}(T_{\mathcal{M}})$, after a period of $\mathcal{M}$, that is,

$$\vec{\epsilon}(T_{\mathcal{M}}) = \mathcal{F}\vec{\epsilon}(0). \tag{22}$$

The Floquet matrix of a Hamiltonian system is real and symplectic, so the Floquet eigenvalues λ come in quadruplets, λ, $1/\lambda$, $\bar{\lambda}$, $1/\bar{\lambda}$. The necessary condition for the stability of the solution is that all the eigenvalues lie on the unit circle of the complex plane, $|\lambda|=1$.

To illustrate the Floquet analysis of (p,q) resonant solutions of the NLS lattice (7), we now obtain the Floquet spectrum of modulational instabilities of a (p,q) resonant plane wave,

$$\Phi_n(t) = A\exp i(kn - \omega t). \tag{23}$$

(The modulational instabilities of plane wave solutions of nonlinear lattices have been analyzed in Refs. 28 and 29.)

One has to investigate the evolution of small perturbations, in both amplitude and phase, of the plane wave

$$\Phi_n(t) = (A + I_n)\exp i(kn - \omega t + \varphi_n), \tag{24}$$

where we assume that the perturbation parameters are small compared with those of the plane wave solution. Introducing expression (24) in (7) and considering the following form for the perturbations $\{I_n, \varphi_n\}$,

$$I_n(t) = I\exp i(Qn - \Omega t),$$

$$\varphi_n(t) = \varphi\exp i(Qn - \Omega t), \tag{25}$$

we obtain the dispersion relation for the perturbation parameter Ω:

$$\begin{aligned}[\Omega - 2(1+\mu A^2)\sin k\sin Q]^2 &= 16(1+\mu A^2)\sin^2 Q/2\cos k[(1+\mu A^2)\sin^2 Q/2\cos k \\ &\quad - \mu A^2\cos k - \nu A^2].\end{aligned} \tag{26}$$

From the above expression one derives the values of $\Omega(A,Q,k;\nu,\mu)$ for the modulational perturbations. When the parameter Ω has a nonzero imaginary part, i.e., the right-hand side of (26) is negative, the plane wave (A,k) becomes unstable under the corresponding modulational (Q) perturbation, whose amplitude will grow exponentially fast in the linear regime (tangent space).

Modulational perturbations (25) correspond to eigenvectors $\{I_n, \varphi_n\}$ of the Floquet matrix:

$$I_n(t + T_{\mathcal{M}}) = \exp(-i\Omega T_{\mathcal{M}})I_n(t), \tag{27}$$

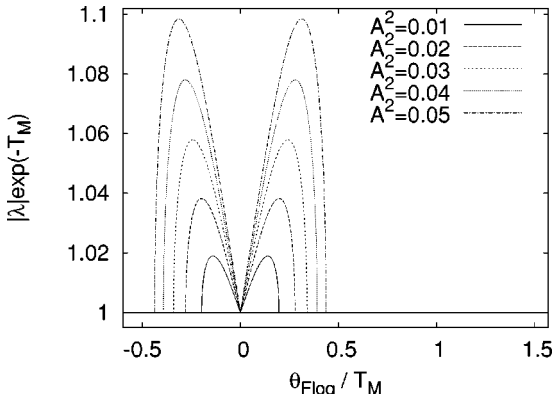

FIG. 3. Plot of the modulus of the unstable Floquet eigenvalues $|\lambda|$ [corresponding to the positive values of $\Im(\Omega)$ in Eqs. (31) and (32)] versus the Floquet angle, θ_{Floq}. Both quantities are conveniently normalized to the period of the map $T_{\mathcal{M}}$. The amplitude of the excursion of $|\lambda|$ and the range of values of θ_{Floq} for which $|\lambda|>1$ grow as the amplitude A of the plane wave is increased. The parameters in Eq. (7) are $\mu=\nu=0.5$ and the wave number of the plane wave is $k=0.5$.

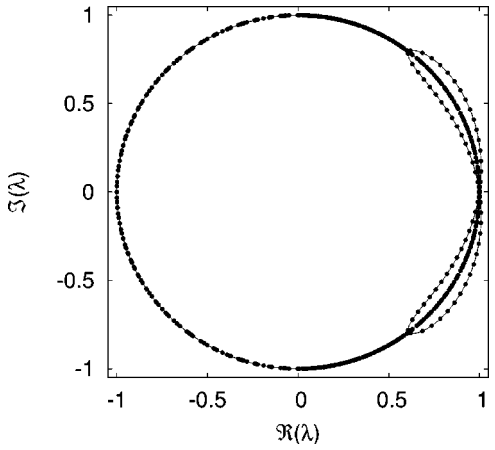

FIG. 4. Plot of the Floquet spectra of a plane wave with modulational instability (circles) and the theoretical prediction (lines) for the distribution of the Floquet eigenvalues in the complex plane given by Eqs. (31) and (32). The amplitude and wave number of the plane wave are $A=0.1$ and $k=0.1\cdot 2\pi$; the nonintegrable parameter value is $\nu=0.1$ and the lattice size is of 400 sites.

$$\varphi_n(t+T_{\mathcal{M}}) = \exp(-i\Omega T_{\mathcal{M}})\varphi_n(t), \tag{28}$$

with associated Floquet eigenvalues $\exp(-i\Omega T_{\mathcal{M}})$. The real part of Ω gives the angle in the complex plane,

$$\theta_{Floq} = -\Re(\Omega)T_{\mathcal{M}}, \tag{29}$$

while the imaginary part $\Im(\Omega)$ gives the modulus of the Floquet eigenvalue,

$$|\lambda| = \exp(\Im(\Omega)T_{\mathcal{M}}), \tag{30}$$

thus providing the information about the linear stability of the solution.

The distribution of angles and moduli in the Floquet spectrum of the modulational instability can be obtained from Eq. (26) by taking the real and imaginary parts of Ω:

$$\Re(\Omega) = 2(1+\mu A^2)\sin k \sin Q, \tag{31}$$

$$\Im(\Omega)^2 = -16(1+\mu A^2)\sin^2 Q/2 \cos k[(1+\mu A^2) \times \sin^2 Q/2 \cos k - \mu A^2 \cos k - \nu A^2]. \tag{32}$$

In Fig. 3 we represent the modulus of the unstable eigenvalues as a function of the Floquet angle for the spectrum of a (p,q) resonant plane wave, taken as an example to visualize the non-point-like character of the instability in the Floquet spectrum in the thermodynamic limit. Note that there is no plane wave harmonic instability ($\theta_{Floq}=0$) due to this mechanism of modulational instabilities.

A numerical computation of the Floquet spectrum of a plane wave (with arbitrary wave number) of a lattice of $N=400$ sites, with periodic boundary conditions, is shown in the complex plane representation of Fig. 4. The instability globes, at angles symmetrically placed around zero in this figure, nicely fit the theoretical (thermodynamic limit) values obtained from Eqs. (31) and (32).

III. MOBILE DISCRETE SCHRÖDINGER BREATHERS

In this section, we show the numerical results on mobile discrete Schrödinger breathers in the NLS lattice (7). These numerics are computed using the tools explained in the previous section. The Newton fixed point continuation requires a good initial guess (meaning that the starting initial conditions have to be in a small neighborhood of the fixed point). Very close to $\nu=0$, the A-L solitary traveling waves (exact solutions at $\nu=0$) provide good starting points. After convergence to the fixed point, we increase adiabatically the value of the parameter ($\Delta\nu=10^{-3}$), and start iteration from the previous fixed point.

An important step in the numerical method used here is obtaining a basis for the subspace of (tangent space) vectors with Floquet eigenvalue +1. These are associated to those degeneracies (symmetries) that one has to eliminate in order to regularize the linear system at each (Newton) iteration step when numerically converging to the fixed point solution.

Away from the A-L limit, it is known (as reported, e.g., in Ref. 30) that only two conserved quantities remain generically as dynamical invariants, the Hamiltonian (8) and the norm (9). They are respectively associated to the continuous time translation and gauge (global phase rotation) invariance. Using the notation $u_i=\Re(\Phi_i)$ and $v_i=\Im(\Phi_i)$, one easily obtains that $(\delta u_i(t)=\dot{u}_i(t), \delta v_i(t)=\dot{v}_i(t))$ is the perturbation associated with time translational invariance, while $(\delta u_i(t)=v_i(t), \delta v_i(t)=-u_i(t))$ is the one with gauge invariance. These are, consequently, Floquet eigenvectors with associated eigenvalue +1, and we can easily check that they coincide with the (two) basis vectors provided generically (i.e., except at special bifurcation values of the parameter, see Sec. III C) by the numerical singular value decomposition (20) explained in the previous section.

In Sec. III A we summarize our findings on the generic structure of mobile Schrödinger discrete breathers. For this, as explained earlier, we have explored particular values for the integers (p,q) and performed continuation of (p,q) resonant A-L traveling waves. The variation of the main structural characteristics of the fixed points along the continuation parameter ν is examined in detail in Sec. III B, for both signs of this parameter. Of particular interest are the observed dras-

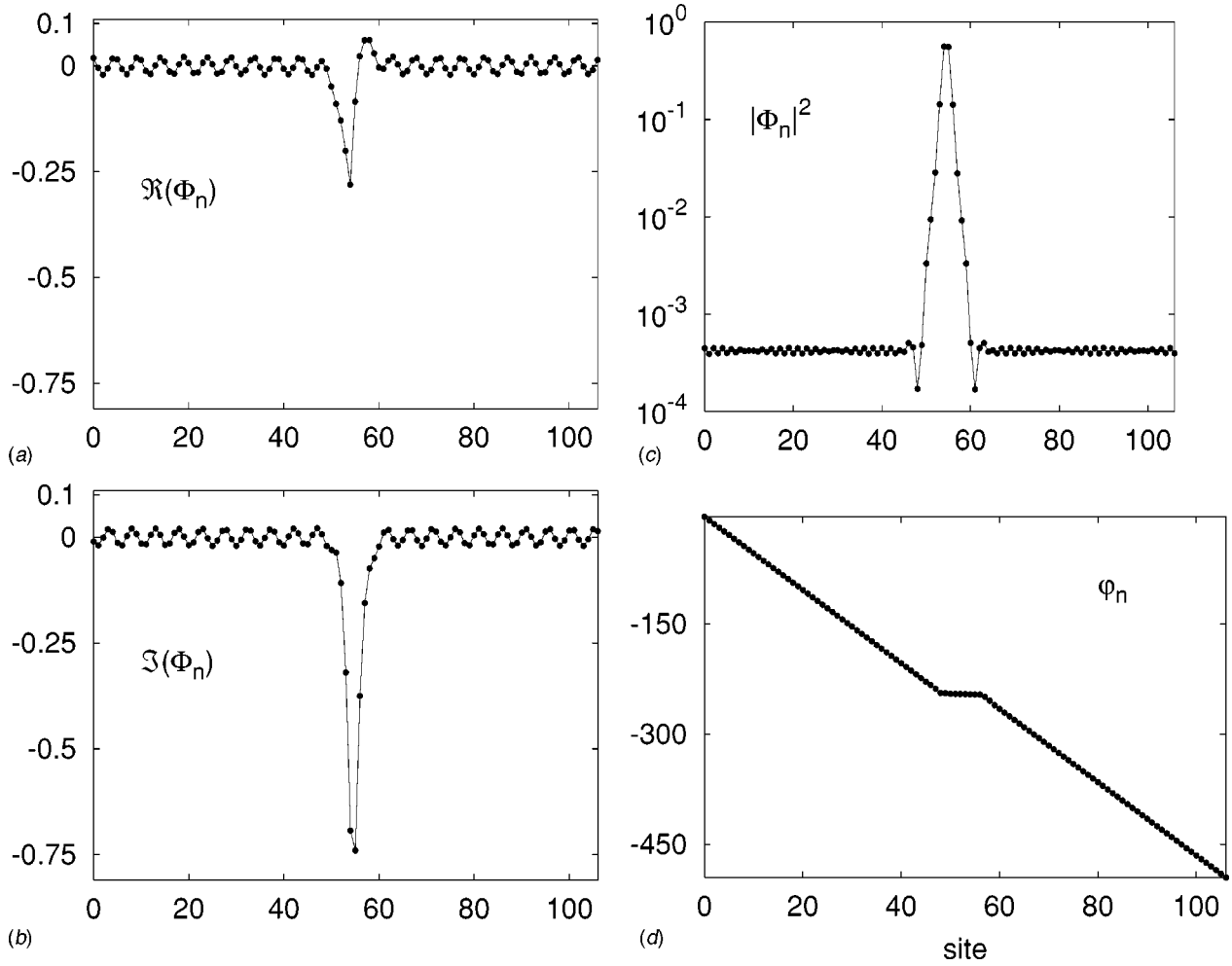

FIG. 5. Instantaneous profile of a (1,1) resonant breather with $\omega_b=2.678$ and $v_b=0.426$; the nonintegrable parameter is $\nu=1.0$ (standard DNLS equation). (a) Real part, (b) imaginary part, (c) modulus and (d) phase. The resonant condition for the harmonic composition of the background gives the contribution of three plane waves. The existence of these plane waves is revealed by the modulation of the extended tail in the modulus profile (c).

tic changes in the structure for $\nu\simeq -0.3$ and $\nu\simeq -0.39$. Then, in Sec. III C, we show the main conclusions on the stability analysis of the mobile Schrödinger discrete breathers, in a sector of the breather parameter space.

A. The structure of the solution

In Fig. 5 we plot the spatial profile of a (1,1) mobile Schrödinger discrete breather for nonintegrability parameter value $\nu=1.0$, and $\omega_b=2.678$.

A quick inspection of this figure provides a first glance of the general structure of the computed (p,q) resonant solutions: The fixed point $\hat{\Phi}$ is the superposition of an (exponentially) localized oscillation (the *core*) moving on top of an extended *background:*

$$\hat{\Phi}=\hat{\Phi}_{core}+\hat{\Phi}_{backg}. \tag{33}$$

In other terms, far away from the core localization site n_0, the solution does not tend to the rest state $\hat{\Phi}_n=0$, but to an extended excited state of the lattice, i.e., for $|n-n_0|\gg 1$,

$$\hat{\Phi}_n(t)=(\hat{\Phi}_{backg})_n(t)\neq 0. \tag{34}$$

One easily realizes (for example, consider a site very far from n_0) that the background has to be itself (p,q) resonant. This can be quickly checked in our numerics: Indeed, the power spectrum $S(\omega)=|\int_{-\infty}^{\infty}\Re[\hat{\Phi}_n(t)]\exp(i\omega t)dt|^2$ at a site n far from n_0 reveals a finite number of s peaks ω_j, $j=0,\ldots,s-1$; one can check that each ω_j numerically fits to a branch of (p,q) resonant plane waves [see Eq. (15)]; this provides a set of amplitudes A_j, and finally one confirms that the superposition of the (A_j,ω_j) plane waves fits the numerical solution $\hat{\Phi}_n(t)$.

While immobile discrete breathers can be described as a sort of homoclinic (and time periodic) connection on the rest state, the mobile localized core instead *connects* a specific linear superposition of low amplitude nonlinear plane waves. One could say that the localized core needs for its motion to "surf over" a specific extended state of radiation:

$$(\hat{\Phi}_{backg})_n(t)=\sum_{j=0}^{s-1}A_j\exp i(kn-\omega_j t). \tag{35}$$

We note that among the members of the (s-parameter) continuous family of (p,q) resonant plane waves (see Sec. I), the fixed point solution contains only a particular member

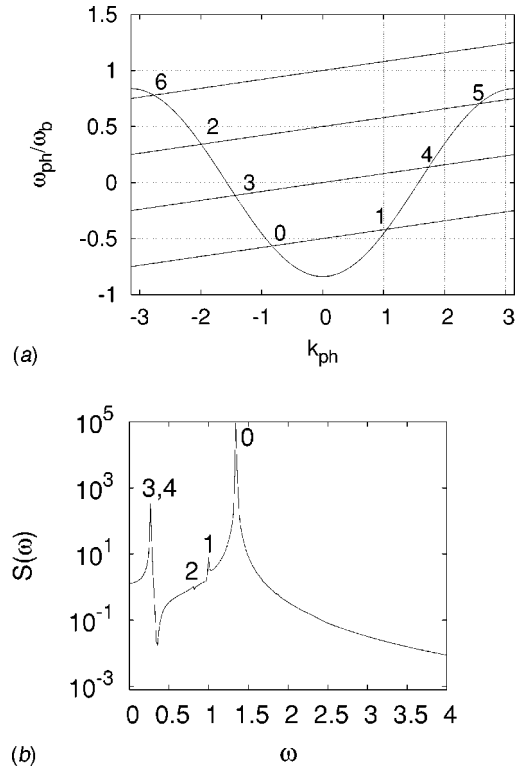

FIG. 6. (a) Plot of the graphical solving of the resonant condition (in the $A_j \to 0$ limit) for a (1,2) resonant breather with $\omega_b = 2.384$ and $v_b = 0.189$. (b) Power spectrum $S(\omega)$ of the background of this solution at $\nu = 1.0$. From (a) Eq. (17) gives the contribution of seven plane waves ($j = 0, \ldots, 6$) but only five ($j = 0, \ldots, 4$) of them are visible due to the difference of orders of magnitude between the amplitudes $|A_j|$. The agreement between the resonant condition equation (for the fitted value of A_j) and the frequencies observed in $S(\omega)$ is up to machine accuracy.

(A_j, ω_j) from each branch [see Fig. 6(a)]. This selection varies smoothly with the (adiabatic) continuation parameter ν. In particular, the amplitude modulus $|A_j|$ selected increases smoothly from its zero value at the integrable limit ($\nu = 0$), for both signs of ν.

If the bare core of a fixed point solution (i.e., after substraction of the background) is taken as initial condition for a direct numerical integration of the equations of motion, one observes radiative losses, along with the corresponding changes in shape, velocity, etc. of the localized moving core. The motion of the bare localized core (not anymore a solution) excites extended states of the lattice. Thus, regarding the exact fixed point solution, one could say that radiative losses of the running core are *exactly* cancelled out when the localized core runs, with specific velocity, on top of the specific linear combination of (A_j, ω_j) resonant plane waves (35).

A complementary numerical observation is the following: Taking as initial condition for a direct integration of the equations of motion (7), a superposition of an immobile discrete breather and the background of a (p,q) resonant mobile breather, it evolves into a moving discrete breather, with approximate velocity $v_b = (p\omega_b)/(2\pi q)$. One thus would say that the background promotes breather translational motion with adequate velocity. In the next section, a connection between background characteristics and the particle perspective (i.e., the Peierls–Nabarro barrier of collective variable theories) will be established, further illuminating the physical description of discrete breather mobility.

Whatever physical perspective one may prefer, the numerical fact is that the generic structure of the fixed point solution is given by the superposition (33). Not too far from $\nu \simeq 0$, where the amplitudes A_j of the fixed point background have small values, one can carefully check that if the bare core is given as a starting guess for Newton iteration, this converges well to the exact complete solution (core + background), by developing the specific selection of A_j amplitudes. This confirms the robustness of the numerics.

Though previous observations of nondecaying tails of numerically accurate mobile discrete breathers in Klein–Gordon lattices[20] and/or (solitary) traveling waves[31] in self-focusing equations had been reported (see also the interesting discussions on this issue in Refs. 21 and 32), no systematic study of those tails is known to us. However, we clearly see that they are an essential part of the exact solution. As argued in the introductory section, the translational motion of a discrete breather introduces a new time scale. In a nonintegrable context, this fact unavoidably implies resonances with plane wave band spectra, and an exact self-sustained moving DB solution could only exist on top of a developed resonant background. This seems to have been (with a few exemptions) not fully appreciated in most of current literature on mobile breathers, where the background is most often either ignored or deliberately suppressed.

A notable feature of the plane wave content of the background $\hat{\Phi}_{backg}$ is that the amplitude modulus $|A_j|$ in (35) differ by orders of magnitude, i.e., $|A_1| \gg |A_2| \gg |A_3| \gg \cdots$, so that only a few frequencies are dominant for most practical purposes [see Fig. 6(b)]. In other words, the extended background associated to a spatially localized moving core is, in turn, strongly localized in the reciprocal (k-space) lattice. The possible relevance of this observation is further discussed below in the concluding section.

B. The background amplitude

In order to characterize the specific features of the nonintegrable motion of discrete Schrödinger breathers, we focus here on the (perhaps) most remarkable among those features: the background amplitude of the uniquely continued fixed point. How does it evolve along the continuation path in parameter space?

For positive values of ν we have followed the line in parameter space $\mu + \nu = 1$ [see Eq. (7)], while for negative values, we took the path $\mu - \nu = 1$. We do not expect other paths to make important differences. As stated earlier, near $\nu \simeq 0$, the amplitude grows from its zero value (at the integrable limit) for both signs of this parameter, for it is a nonintegrable effect. However, for larger values of nonintegrability $|\nu|$ the background amplitude evolution shows some important differences for the two signs of ν.

In Fig. 7 we plot the background amplitude (modulus) of the (1,1) resonant fixed point versus the continuation parameter ν, for three different values of the breather frequency ω_b. For $\nu > 0$, one observes that the amplitude steadily increases

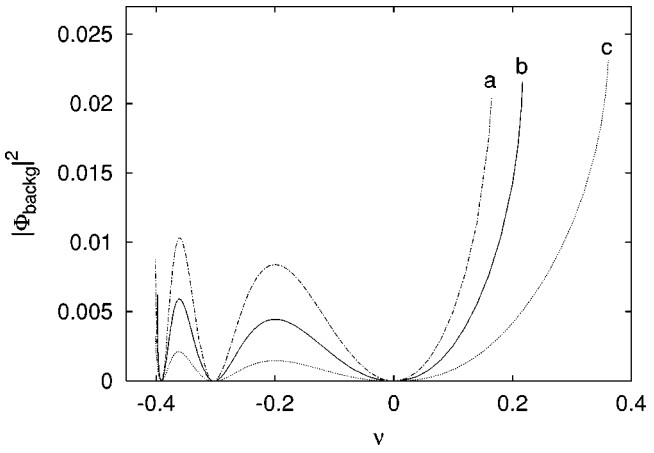

FIG. 7. Background amplitude versus ν for three different (1/1) resonant breathers with frequencies: (a) $\omega_b=5.65$, (b) $\omega_b=4.91$, and (c) $\omega_b=4.34$. Note the two different behaviors: for positive values of ν $|\Phi_{backg}|^2$ is a monotonous increasing function of ν while for the negative part it shows smooth rises and falls.

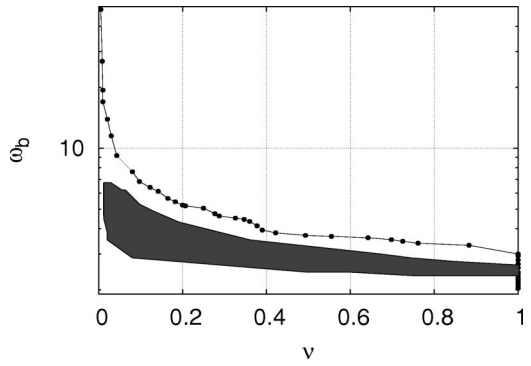

FIG. 8. Continuation diagram of (1,1) resonant breathers as a function of the frequency ω_b. The end of the numerical continuation, $\nu_{\max}(\omega_b)$, is represented by the line with dots. The region where mobile breathers suffer from core instabilities is limited by the shaded area.

with ν before continuation stops (i.e., Newton iteration ceases to converge beyond a certain maximum ν value). Note that the amplitude grows faster for higher values of the frequency, and that the continuation stops (correspondingly) at a smaller value of ν. This may suggest that the failure of fixed point continuation is related to a somewhat excessive growth of the background amplitude, an issue that will be discussed later.

For $\nu<0$, after an initial growth the background amplitude decreases down to almost negligible values around $\nu \simeq -0.3$, then grows and again decreases close to zero at $\nu \simeq -0.39$, and so on, in progressively narrower intervals with larger peak amplitude, until continuation stops. Most noticeable is the fact that the intervals neither depend on the breather frequency ω_b nor on the breather velocity v_b. Why do background amplitudes decay so dramatically at those regions in parameter space? An important hint is presented in the next section, where the Floquet stability analysis of immobile discrete breathers will show a coincident situation of mirror-symmetry breaking (and its absence for positive ν values).

For other values of p and q that we have numerically investigated, the same features of the background amplitude variation as shown in Fig. 7 are qualitatively reproduced.

C. Floquet analysis

On the basis of the general arguments given in Refs. 27 and 33, the Floquet spectra of immobile DB in the thermodynamic limit, $N\to\infty$, consists of two components: the (continuous) Floquet spectrum of the asymptotic state of the solution (rest state), and a discrete part associated with spatially localized eigenvectors. The continuous part is composed of small amplitude (linear) plane waves, the so-called phonons. However, for mobile DB the asymptotic state of a (p,q) resonant fixed point solution is a superposition of plane waves, the background $\hat{\Phi}_{backg}$. From this, one should expect the Floquet spectrum of a (p,q) resonant DB being composed of two components: the discrete (spatially localized) eigenvectors and a continuous part associated with the linear stability of the background plane waves. The continuous part of the Floquet spectrum should reflect the same results of the modulational instabilty analysis of Sec. II C. In particular, this means that any modulational instability a plane wave may suffer will be also an instability of a fixed point solution whose background contains this plane wave. In the future we will refer to any instability of the continuous part of the Floquet spectrum as *background instability.* Any instability from the discrete part is a *core instability.*

First we focus on *core instabilities.* For this we turn attention to the continuation of mobile (p,q) resonant breathers. Figure 8 shows in the $\nu-\omega_b$ plane (dotted line) the values $\nu_{\max}(\omega_b)$ where the numerical continuations stop due to nonconvergence of Newton iteration for $p=1$, $q=1$ and $\nu>0$. As was remarked above, the continuation stop is associated with the rapid increase of the background amplitude shown in Fig. 6. Only low frequency breathers, for which the background amplitude increases more slowly, can be numerically continued all the way to the standard DNLS equation. The linear stability analysis of (p,q) resonant breathers yields a well defined region in the $\nu-\omega_b$ diagram where *core instabilities* appear. There is an island inside the continuation region of Fig. 8, where the Floquet spectra contain a real eigenvalue $\lambda>1$. We observe the evolution of this Floquet eigenvalue (and its complex conjugate) as the parameter ν is increased in Fig. 9(a), for a (1,1) breather of frequency $\omega_b=2.678$. Here the angle (θ_{Floq}) in the complex plane is plotted versus ν. The interval of constant zero angle corresponds to the section (constant ω_b) of the instability island in Fig. 8.

Along the whole continuation path, the profile of the corresponding unstable eigenvector is localized. An example of this profile inside the instability island is shown in Figs. 9(b) and 9(c), where one observes that the localized instability shows a decaying background along the direction opposite to the motion. The decay rate increases as the modulus of the eigenvalue grows and decreases again when λ returns to the unit circle. On the other hand, the stable Floquet eigenvector associated with $1/\lambda$ shows a wing decaying along the mirror symmetric direction. The direct integration of the equation of motion reveals that the unstable solution experiences a pinning after a transient of regular motion with ve-

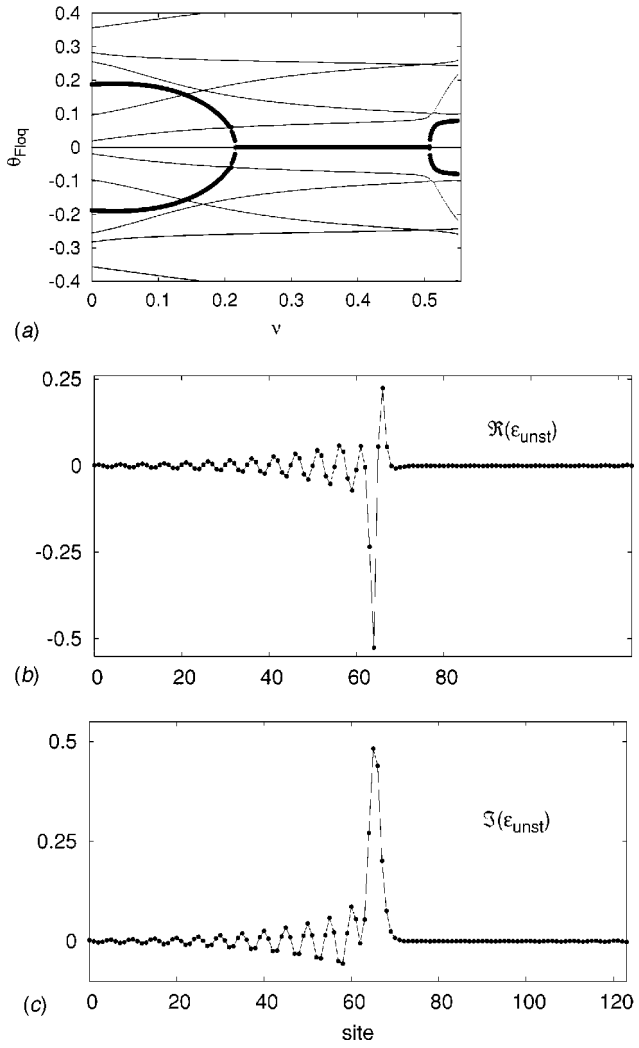

FIG. 9. (a) Floquet angle evolution of the spectra of a (1,1) resonant breather with $\omega_b=2.678$. The thick trajectory corresponds to the localized eigenvector that becomes unstable ($\theta_{Floq}=0$ interval). Instantaneous profile of the real (b) and imaginary (c) parts of the Floquet unstable eigenvector of a (1,1) breather with $\omega_b=3.207$ and $\nu=0.26$. The decaying tails along the direction opposite to the motion reveals the energy loss that the unstable eigenvector causes to the solution.

locity $v_b=p/(qT_b)$. After the solution pins at site n, its core center oscillates around this site. The trapping of the unstable MB could be interpreted as a result of the energy losses that the growth of the linearly unstable perturbation induces on the solution.

Returning to the instability island shown in the diagram of Fig. 8, some final observations are worth summarizing: (i) there is a range of frequencies where mobile breathers of the standard DNLS equation ($\nu=1$) suffer from this instability; (ii) very high frequency breathers do not experience this instability (in the short range where they can be continued); and (iii) very low frequency breathers are stable all the way up to $\nu=1$.

We turn now to *background instabilities.* Once we know the plane wave content $(k_0,k_1,\ldots)$ of a (p/q)-resonant fixed point, we can know whether the solution is subject to MI or not and, if it is unstable, what are the harmful perturbations (Q). This problem is not so simple because we cannot know

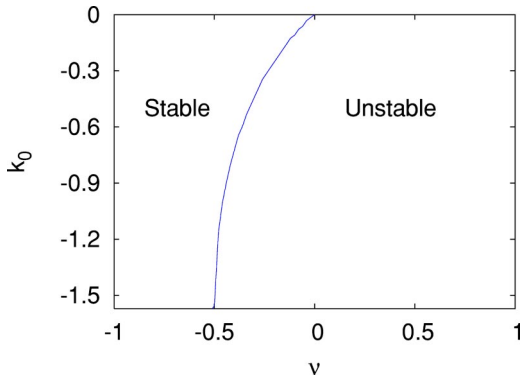

FIG. 10. (Color online). Modulational instability existence diagram for a plane wave with wave number $k_0\in[-\pi/2,0]$. This diagram fixes the region where mobile discrete breathers with a background composed of only one plane wave do not suffer from background instability.

a priori the plane wave content if we do not have the amplitudes of each one (17). However, we can derive a necessary condition for not having MI if we consider that, from (17), the background is always composed of at least one plane wave $(m=0)$ with k_0 between $[-\pi/2,0]$. From this we can simplify the analysis of the background stability to the k_0 plane wave stability as a necessary condition for the MB stability. For this we calculate, for each ν and k, the value of the right-hand side of (26) for all the range of $Q([-\pi,\pi])$ and A. If this value is always positive, the plane wave with this k_0 is free from modulational instabilities at this point of the model (7) with parameter ν. From this extensive exploration we obtain, see Fig. 10, the region in the $k-\nu$ plane where MI is present.

In the range of ν between $[-1,-0.5]$ there is no modulational instability for single plane waves of any value of k between $[-\pi/2,0]$, and in particular for k_0. However, this does not guarantee that moving breathers are free from these instabilities in this region, unless the background has only one plane wave (as is sometimes the case). On the contrary, in the region $\nu>0$ any moving breather suffers such instabilities. The transition area in the region $\nu\in[-0.5,0]$ presents MI depending on which k_0 we have. For the range where no plane wave with k between $[-\pi/2,0]$ is subject to MI we can assure that if there is only one contribution, k_0, to the background, the corresponding MB solution is stable. For example, this is the case for $(1/1)$ resonant breathers if $\omega_b>4$ and for $(1/2)$ resonant breathers if $\omega_b>8.46$. The Floquet spectra of a moving breather satisfying these requirements is plotted in Fig. 11(c).

After the analysis of both types of instabilities eventually experienced by moving Schrödinger breathers, we finally report on a most relevant numerical fact revealed by the Floquet analysis of the family of *immobile discrete breathers* for $\nu<0$: Near $\nu\simeq-0.3$ an immobile two-site DB experiences a mirror symmetry-breaking (pitchfork) bifurcation becoming linearly unstable. When approaching the bifurcation point, two conjugate Floquet eigenvalues quickly approach +1, where they meet, and then separate along the real axis. The eigenvector associated to the unstable $\lambda>1$ Floquet eigenvalue is localized and odd-symmetric, and is termed the

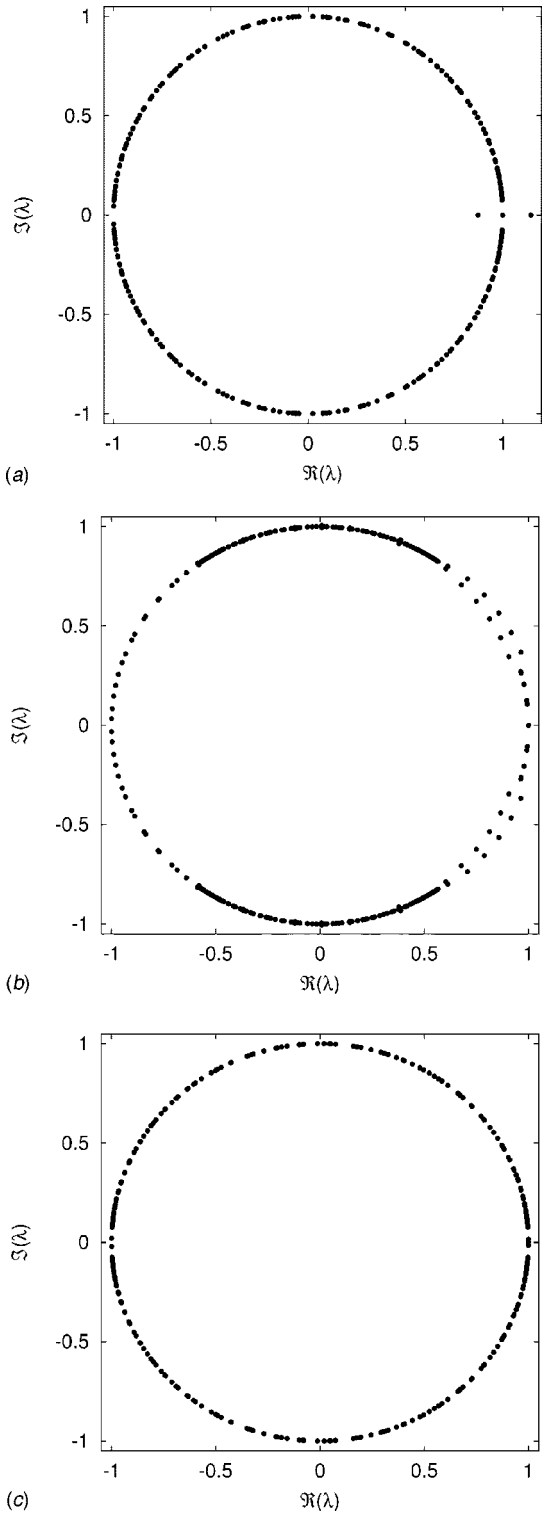

FIG. 11. Floquet spectra of (1,1) resonant breathers: (a) for $\omega_b=4.348$, $v_b=0.692$ and $\nu=0.08$ the spectra shows the core (localized) instability; (b) for $\omega_b=6.610$, $v_b=1.052$ and $\nu=0.07$ the spectra shows the background (modulational) instability [also present but not visible in (a)]; and (c) for $\omega_b=4.348$, $v_b=0.692$ and $\nu=-0.39$ the solution is linearly stable.

symmetry-breaking or depinning mode ϕ^{dep}. We recall here that the background of an immobile breather is the rest state $\hat{\Phi}=0$, whose continuous spectrum consists of small amplitude (linear) plane waves. The depinning mode, on the other hand, is a localized core instability of the immobile breather, favoring a translation of the core center. For a smaller value of $\nu\simeq-0.39$ there is another symmetry-breaking bifurcation where the two-site breather becomes stable, again interchanging the stable character with the one-site. The corresponding bifurcation diagram for these two symmetry breaking transitions is plotted in Fig. 12.

In the first symmetry breaking bifurcation, two unstable mirror-asymmetric immobile breathers emerge from the bifurcation point, progressively evolve toward the (stable) two-site breather, and finally collide in a new pitchfork bifurcation from where an unstable two-site breather emerges. The net result is an inversion of stability between one- and two-site immobile breathers. Around the narrow interval of ν values where these two bifurcations occur, the energies of the three types of breathers involved (one-site, two-site, and asymmetric) have very small differences. From a particle perspective, this should make the breather motion easier. It is precisely in this same narrow interval where (see Sec. III B) we observe that the background amplitude of moving breathers becomes negligible. This is not a coincidence as we will argue in Sec. IV.

IV. PARTICLE PERSPECTIVE ON DISCRETE BREATHERS

The appealing framework and success of collective variable approaches (see, e.g., Refs. 34–38) to the problem of nonintegrable motion of discrete breathers rely on the fidelity of a particlelike description of these field excitations that they provide. In these approaches, the effective dynamics of only a few degrees of freedom (e.g., the localization center, and the spatial width of the state, etc., in some instances[12]) replaces the whole description of the moving localized state.

Though unable to account for all the nonintegrable features, perturbative collective variable theories of NLS lattices provide a sensible physical characterization of important features of the nonintegrable mobility of localized solutions, like the emergence[39] of a Peierls–Nabarro barrier to motion. Here we summarize the main results of this particlelike description and compare them with the behavior of numerically exact (p,q) resonant moving breathers. Our goal is twofold: to acquire a correct physical understanding of the numerical facts, and then to make an assessment of validity and intrinsic limitations of collective variable approaches.

A. Collective variables theory

A presentation of the particle perspective on moving Schrödinger breathers near the A-L integrable limit can be found in Ref. 36 (see also Refs. 34, 35, 37, and 38), where the interested reader will find the relevant formal aspects of the theory.

Using the integrable solitary wave (4) as an ansatz for the moving breather solution in the perturbed A-L lattice, $\nu\neq0$ and small in (7), one considers the parameters α, β, x_0 and Ω as dynamical variables (variation of constants). The time evolution of these parameters in the perturbed lattice is governed by

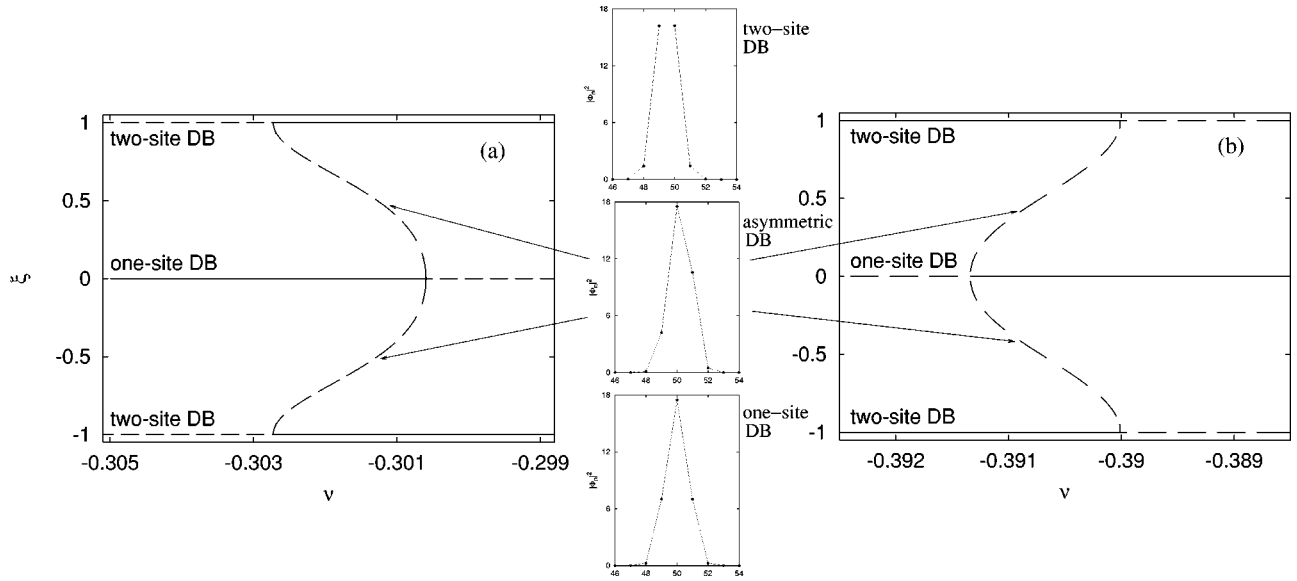

FIG. 12. Graphical representation of the two first *symmetry breaking bifurcactions* for $\nu<0$. The quantity ξ in the vertical axes of both figures is defined, referred to the one-site breather, as the difference between the modulus $|\Phi|$ of the two sites adjacent to the maximum ($|\Phi_{\max}|$), i.e., $\xi\sim|\Phi_{\max-1}|-|\Phi_{\max+1}|$. For the one-site DB $\xi=0$ and for the two-site DB $\xi=1$, for this ξ is conveniently normalized with the difference between $\Phi_{\max}$ and $\Phi_{\max\pm1}$. The continuous lines represent the regions where the static solutions are linearly stable while the discontinuous ones represent the unstable regions. The modulus profiles of the three immobile coexisting solutions are plotted in the central insets for $\omega_b=6.215$ and $\nu=-0.3012$.

$$\dot{x}_0 = 2\sin\alpha\frac{\sinh\beta}{\beta}, \tag{36}$$

$$\dot{\Omega} = 2\cos\alpha\cosh\beta + \alpha\dot{x}_0 + g(\beta), \tag{37}$$

$$\dot{\beta} = 0, \tag{38}$$

$$\dot{\alpha} = -\nu\sum_{s=0}^{\infty}\frac{8\pi^3\sinh^2\beta}{\beta^3\sinh(\pi^2 s/\beta)}\sin(2\pi s x_0), \tag{39}$$

where

$$g(\beta) = 2\nu\left[\frac{2\sinh\beta\cosh\beta}{\beta} - \frac{\sinh^2\beta}{\beta} - 1\right] + \nu\sum_{s=1}^{\infty}4\pi^2\cos(2\pi s x_0)\left[\frac{\sinh^2\beta\cosh(\pi^2 s/\beta)\pi^2 s}{\beta^4\sinh^2(\pi^2 s/\beta)} - \frac{2\sinh^2\beta}{\beta^3\sinh(\pi^2 s/\beta)} + \frac{2\sinh\beta\cosh\beta}{\beta^2\sinh(\pi^2 s/\beta)}\right]. \tag{40}$$

These relations can be viewed as the Euler–Lagrange equations of the collective variable Lagrangian obtained in Ref. 36. The variation of the breather parameters gives the evolution of solution (4) for the perturbed A-L equation. Furthermore, one can regard Eqs. (36) and (39) as the Hamilton equations for the canonical conjugate variables x_0 and α of the following effective Hamiltonian:

$$\mathcal{H}_{\text{eff}} = \mathcal{T}_{\text{eff}} + \mathcal{V}_{\text{eff}} = -2\cos\alpha\frac{\sinh\beta}{\beta} - \nu\sum_{s=1}^{\infty}\frac{4\pi^2\sinh^2\beta}{\beta^3\sinh(\pi^2 s/\beta)}\cos(2\pi s x_0). \tag{41}$$

This effective Hamiltonian dictates the dynamics of the position of the solitary wave. Note that the (collective) variable β is an invariant of motion, so it enters as a parameter into the effective Hamiltonian, and that the time-average value of $\dot{\Omega}$ (the parameter ω_b of the integrable solitary wave, now a function of time) is an increasing function of this parameter β. The effective potential $\mathcal{V}_{\text{eff}}$ acts as a barrier to the displacement motion (x_0 variations) and is naturally related to the Peierls–Nabarro potential. The amplitude of this barrier is an increasing function of both the nonintegrability parameter $|\nu|$ and β. The equilibrium points (representing immobile breathers) of this potential are $x_0=n$ and $n\pm\frac{1}{2}$ with n an integer. For $\alpha=0$, the former are stable (centers) one-site breathers, while the latter are unstable (saddle) two-site breathers; for the case $\alpha=\pi$ (staggered breathers) the stability is reversed.

A remarkable further consequence is the following:[35] *there are no perturbative traveling wave solutions, for values of ν larger than certain critical value $\nu_{cr}(\beta)$*. In particular, for $\beta>\beta_c\simeq3.6862$, one cannot continue A-L mobile breathers [i.e., $\nu_{cr}=0$ (see also important remarks in Ref. 38)]. This consequence could also be (qualitatively) expected for a class of nonintegrable Schrödinger lattices (for some qualified perturbations of the integrable limit) with on-site nonlinearity. One expects also that lattices with purely intersite

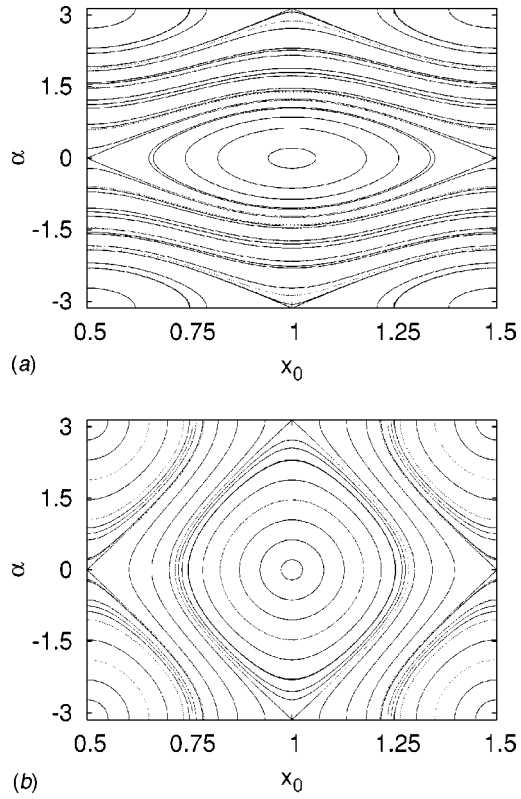

FIG. 13. Collective variable (α, x_0) phase portrait transition for a value of $\beta=3.0$. (a) Shows the phase portrait for $\nu=0.2$ $(<\nu_{cr})$; there are x_0-unbounded trajectories (mobile breathers) coexisting with bounded ones (oscillating breathers). When $\nu=1.0$ $(>\nu_{cr})$ (b) we only have x_0-bounded trajectories: there are no mobile solutions.

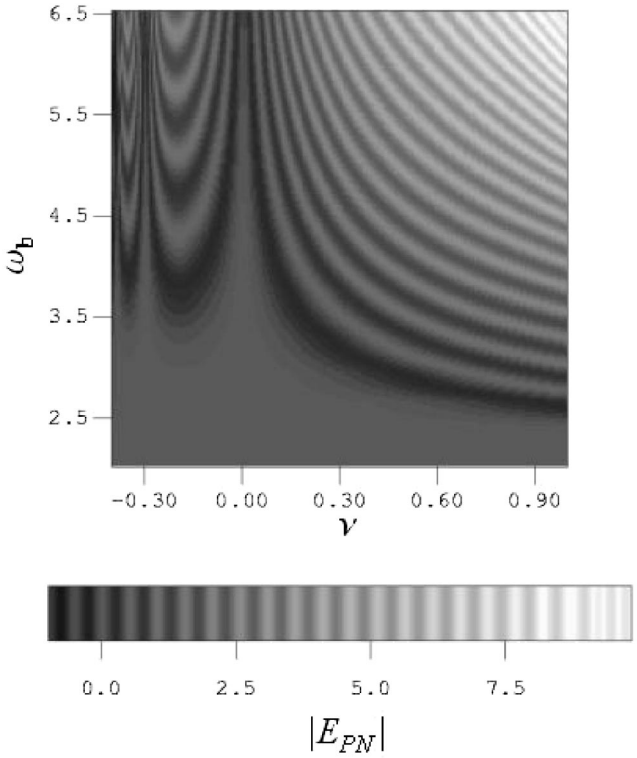

FIG. 14. Density plot of the absolute value of the Peierls–Nabarro barrier, $|E_{PN}|$, as a function of ω_b and ν. For positive values of ν, $|E_{PN}|$ is a monotonous increasing function of ν and ω. For negative values the plot reveals the oscillating behavior of $|E_{PN}|$ as a function of ν (for a given value of ω_b).

(FPU-like) nonlinearity do not show this kind of transition.

In Fig. 13 we plot typical phase portraits at both sides of ν_{cr}. Figure 13(a) shows the dynamics for ν smaller than the threshold value (given by β): there are open trajectories in x_0 corresponding to mobile breathers and closed orbits between the separatrix manifolds corresponding to breathers which oscillate around the equilibrium position of $\mathcal{V}_{\text{eff}}$. Figure 13(b) is the phase portrait after the transition: there are no longer mobile solutions and (besides the oscillating breathers) there are instead open trajectories in α. The transition point, for a given β, occurs when trajectories with rotating α appear, and moving breathers disappear as the effect of separatrix line rearrangement on the cylinder $(x_0, \alpha(\text{modulo}2\pi))$ phase portrait.

Note that the existence of oscillating breathers is a consequence of the existence of a Peierls–Nabarro potential. These breather solutions do not perturbatively continue from the integrable limit. In Sec. IV C we will investigate them and provide further numerical confirmation of the existence of these genuinely nonperturbative solutions, predicted by the collective variables theory.

B. Energy balance governs mobility

In order to correlate collective variable predictions with the numerical results presented in Sec. III one should first realize that our direct numerical approach computes breathers with fixed values of ω_b and v_b and that these parameters are not tied to any specific ansatz. In particular, the connection of these two parameters with the collective variables is given by Eq. (6) in the integrable limit. For the perturbed (near-integrable) lattice, ω_b and v_b are identified as the time averages of $\dot{\Omega}$ and $\dot{x}_0$, respectively.

The Peierls–Nabarro (PN for short) barrier is naturally identified as the energy difference [given by the Hamiltonian (8)] between the two immobile breathers of the same frequency ω_b, one centered at a site n and the other (two-site) at a bond $n\pm\frac{1}{2}$:

$$E_{PN}(\nu,\omega_b) = H(\nu,\omega_b,n) - H\left(\nu,\omega_b,n\pm\tfrac{1}{2}\right). \tag{42}$$

In the integrable A-L limit this barrier is zero due to the degeneracy (continuous translation invariance) of the breather family solution, but for $\nu\neq 0$ this invariance is broken and only these two isolated solutions persist. The energy difference of the two pinned solutions is thus viewed as the minimal extra *"kinetic energy"* of center of mass translation that a mobile breather must incorporate for overcoming the barriers to its motion.

We have studied the behavior of the PN barrier in the Salerno model by continuing immobile breathers, both centered at a site and at a bond, while computing their energy difference. The computations of the barrier are made for a grid of values of ω_b. Figure 14 shows the *"equipotential"* lines of the PN barrier in the (ν,ω_b) plane. The results show different behaviors depending on the sign of ν:

$\nu<0$: Here one observes the effects of the symmetry breaking bifurcations cascade described in Sec. III C. The

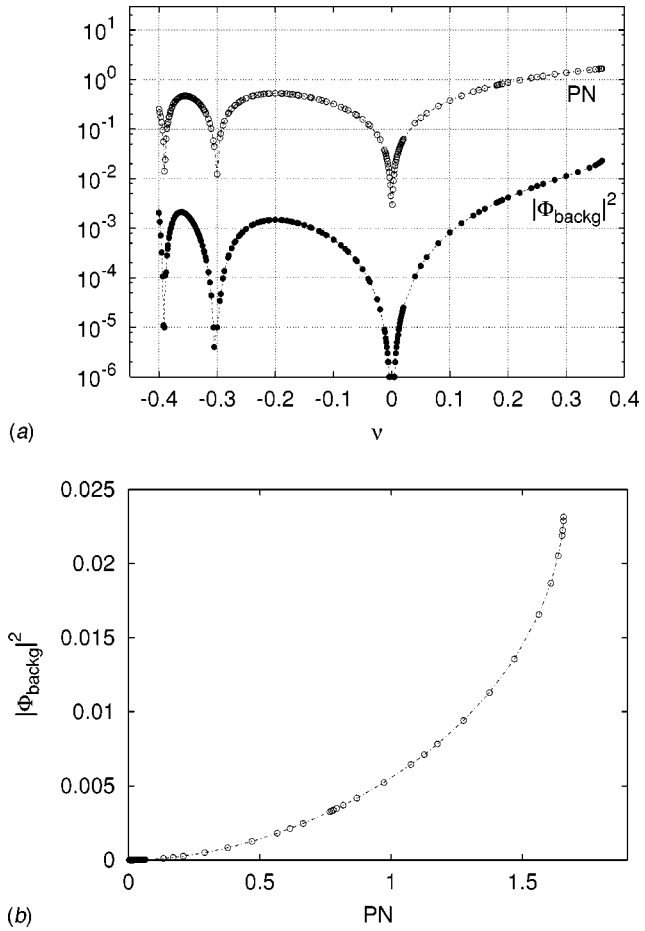

FIG. 15. Peierls–Nabarro barrier $|E_{PN}|$ from immobile breather with $\omega_b = 4.34$ and background square amplitude $|\Phi_{backg}|^2$ for a (1,1) resonant breather of the same frequency ($v_b = 0.691$). In (a) we show both quantities in semi-log scale as functions of ν, illustrating the strong correlation between them for both signs of ν. (b) shows, for positive values of ν, the nonlinear relation between $|\hat{\Phi}_{backg}|^2$ and $|E_{PN}|$. Note the sudden increase of the slope close to the end of numerical continuation.

successive stability inversions between site and bond centered breathers involve a substantial decrease of the Peierls barrier. The appearance of asymmetric solutions in these bifurcations introduces a new energy and, correspondingly, the Peierls barrier is computed as the maximum energy difference between the three pinned solutions: the two symmetric (site and bond centered) and the asymmetric breather.

$\nu > 0$: Here the behavior of the Peierls barrier follows qualitatively the collective variable predictions on the effective potential experienced by the particle. The increasing character, with ν and ω_b, of the numerical barrier is qualitatively the same as that predicted from V_{eff} (as a function of ν and β) by the theory.

The PN barrier of (ω_b) immobile breathers and the background amplitude of $(\omega_b, v_b = p\omega_b/2\pi q)$ mobile breathers are in fact strongly correlated. This correlation is obtained considering the functions $|E_{PN}|(\nu)$ and $|\hat{\Phi}_{backg}|^2(\nu)$. Both functions are plotted for a fixed value of $\omega_b = 4.34$ in Fig. 15(a). The behavior of $|E_{PN}|(\nu)$ for negative ν (revealing the cascade of bifurcations explained before in Sec. III C) is closely followed by $|\hat{\Phi}_{backg}|^2(\nu)$ with the corresponding sequence of growths and decays. The strong correlation holds also for positive values of ν, where numerical PN barrier data are available for a larger interval of ν values (due to the absence of the symmetry breaking cascade of bifurcations). Indeed, the correlation is so strong that one is tempted to view the PN barrier and the background amplitude as complementary aspects of a single phenomenon: the breaking of the continuous translational invariance, and the associated lack of core momentum conservation.[40] Indeed, the background amplitude of moving breathers is a monotone increasing function of the PN barrier of pinned breathers of the same frequency, as shown in Fig. 15(b), where $|\hat{\Phi}_{backg}|^2(|E_{PN}|)$ is plotted.

However, we also observe clearly in Fig. 15(a) that, when the continuation end is approached, the rate of growth of $|\hat{\Phi}_{backg}|^2(\nu)$ increases dramatically (the concavity of the curve in log scale turns upwards), while the PN barrier does not increase much faster than before. This is reflected in Fig. 15(b), where the slope approaches verticality, indicating that, in this range of E_{PN} values, the background grows rapidly.

This numerical observation suggests taking a closer look at the precise influence of the background amplitude on the core energy variations associated with the existence of PN barriers. To this end, we use the conservation of the Hamiltonian (8) and insert this equation into the form (33) of the (p,q) resonant fixed point. The energy of the solution can be decomposed in the following terms:

$$\mathcal{H}[\hat{\Phi}] = \mathcal{H}[\hat{\Phi}_{core}] + \mathcal{H}[\hat{\Phi}_{backg}] + \mathcal{H}^{int}, \tag{43}$$

where $\mathcal{H}^{int}$ is the interaction energy, i.e., the crossed terms of $\hat{\Phi}_{core}$ and $\hat{\Phi}_{backg}$. Let us now consider the simplest case in which the background has a single resonant plane wave. Along with the total energy, also the energy of the plane wave is a constant in time so that

$$\frac{\partial \mathcal{H}[\hat{\Phi}_{core}]}{\partial t} = -\frac{\partial \mathcal{H}^{int}}{\partial t}. \tag{44}$$

In other words, the variations of the core energy during the motion are exactly compensated by those of the interaction term.

If one takes, as an ansatz for $\hat{\Phi}_{core}$, the A-L solution, one formally obtains for $\mathcal{H}^{core} \equiv \mathcal{H}[\hat{\Phi}_{core}]$ the collective variables Hamiltonian (41). But note that here it would no longer be a constant of motion, due to the interaction with the background. Instead (as P. Kevrekidis suggested to us), we directly compute numerically the evolution of the core energy $\mathcal{H}^{core}$, which in turn determines $\mathcal{H}^{int}$ up to an additive constant.

For this we take a fixed point solution with a single plane wave in its background, and then substract off the plane wave to obtain $\hat{\Phi}_{core}$, from where $\mathcal{H}^{core}(t)$ is computed. In Fig. 16 we have plotted the evolution of the core energy as a function of the localization position (center) of the breather core. The localization center of a lattice function Φ_n is defined using the conserved norm (9):

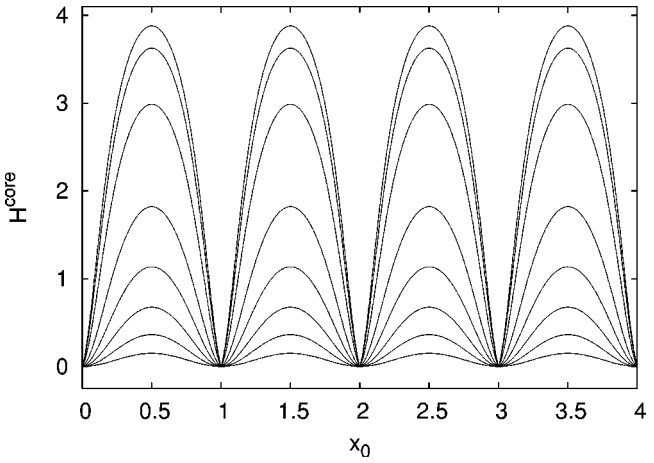

FIG. 16. Plot of $\mathcal{H}^{core}$ of a (1,1) resonant breather as a function of the localization center x_0 for different values of ν. The parameters of the solution are $\omega_b=5.056$ and $v_b=0.805$. The values of ν are 0.04, 0.08, 0.12, 0.16, 0.20, 0.24, 0.25 and 0.2512 (end of the continuation), the amplitude of the oscillation of $\mathcal{H}^{int}$ grows with ν. (The minimum value of $\mathcal{H}^{int}$ has been set to zero in order to compare the different functions.)

$$x_0 = \frac{\sum_n n \ln\left(1+\mu|\Phi_n|^2\right)}{\mu\mathcal{N}}. \tag{45}$$

As expected, the core has extracted the maximum available from the interaction energy (with the background) when the core passes at $n\pm\frac{1}{2}$ (maxima of the PN barrier) and has returned it to the interaction term when at n (minima of the PN barrier).

Another interesting feature of these numerically obtained functions is seen from the variations in the form of the oscillation of $\mathcal{H}^{core}$ as the nonintegrable parameter ν is increased. At the same time, as the energy difference between n and $n\pm\frac{1}{2}$ increases the modulus of the derivative $\partial\mathcal{H}^{core}/\partial x_0$ in the neighborhood of $x_0=n$ also increases. These variations become faster when the end of the continuation is approached, reaching a cuspidal point for the last ν reached. The background amplitude is included in $\mathcal{H}^{int}$, and of course in $\partial\mathcal{H}^{int}/\partial t$; the dramatic variation of it at the end of the continuation could be interpreted in terms of this derivative variation in $x_0=n$.

C. Oscillating breathers

The emergence of the Peierls barrier and the behavior of the background amplitude illustrate the physical interpretation of this background as a (p/q)-resonant energy support to overcome the barrier to motion. We now confirm this statement searching for another kind of solution: *oscillating breathers*. These solutions are predicted by collective coordinates approaches and are a consequence of the loss of translational invariance out of the integrable limit. Following the above interpretation of the background role one can imagine certain solutions with a background amplitude not high enough for surpassing the Peierls barrier and allowing travel along the lattice. In terms of a well defined potential, considering the particle perspective, the center of these localized solutions would be oscillating between $\left(n-\frac{1}{2}\right)$ and $\left(n+\frac{1}{2}\right)$ for the unstaggered ones or between n and $(n\pm1)$ for the staggered ones.

From our perspective, the oscillating breathers are solutions with two frequencies: the internal one of the breather (ω_b) and the one corresponding to the oscillatory motion (ω_{osc}). Once again, we have a problem dealing with two time scales and consequently we have to impose that the two frequencies are commensurate $p\omega_b=q\omega_{osc}$. The fixed point problem is now associated with the map:

$$\mathcal{T}_{qT_b}\Phi_n(t) = \Phi_n(t). \tag{46}$$

We cannot, however, develop the Newton iteration scheme in a similar way as for mobile breathers. There is no longer any family of oscillating breathers providing a good start point for the continuation (they are intrinsic solutions of the nonintegrable regime because they appear as the Peierls barrier emerges). The way to obtain a good *ansantz* (as Cretegny and Aubry already used to find mobile breathers in Klein–Gordon lattices[20]) is to perform a small perturbation of the static solution (pinned at a site n) with the depinning internal mode:

$$\Phi_n^{ansantz} = \Phi_n^{static}(\omega_b) + \epsilon\delta\phi_n^{dep}. \tag{47}$$

The dynamics of the perturbed solution for small enough values of ϵ shows the oscillating behavior expected and for large enough values of ϵ the breather starts to move. Obviously in both cases the motion finishes after a transient due to radiation (they are not exact solutions). Tuning the parameter ϵ we search for those oscillatory transients whose ω_{osc} is resonant with the breather frequency ω_b. The transient is much more stable when the nonintegrable parameter ν is very small, close to the A-L limit. We first search here for a good initial guess for the method and then obtain the exact solution of the map (46). Once the exact solution is obtained for a small ν, we can perform the continuation to higher values in the same way as we did for mobile solutions. In Fig. 17(a) we show the evolution of the amplitude of oscillation as ν is increased from 0.05 to 0.18. The amplitude of the oscillation is represented by the phase portrait of the localization center of the breather defined as in (45). The continuation reflects that the amplitude of the oscillation, for a fixed value of ω_{osc}, grows with ν. In Fig. 17(b) the density plot of $|\hat{\Phi}_n|^2$ is shown as a function of time, revealing the oscillating pattern of the solution.

The existence of exact oscillating breathers is a consequence of the existence of a Peierls barrier. The structure of these solutions reveals the existence of a background (resonant with the map) whose amplitude grows as ν (and consequently the amplitude of oscillation) is increased. This is the picture we expected from the role played by the interaction background–core in the energy balance during motion. The monotonous growing behavior of the background versus the oscillation amplitude strongly suggests that if the amplitude of the former is increased, the solution will be able to translate steadily. This has been checked by direct numerical integration, because no exact solutions connecting the oscillating with the mobile ones can be obtained due to the different maps employed to obtain both types of solutions. However,

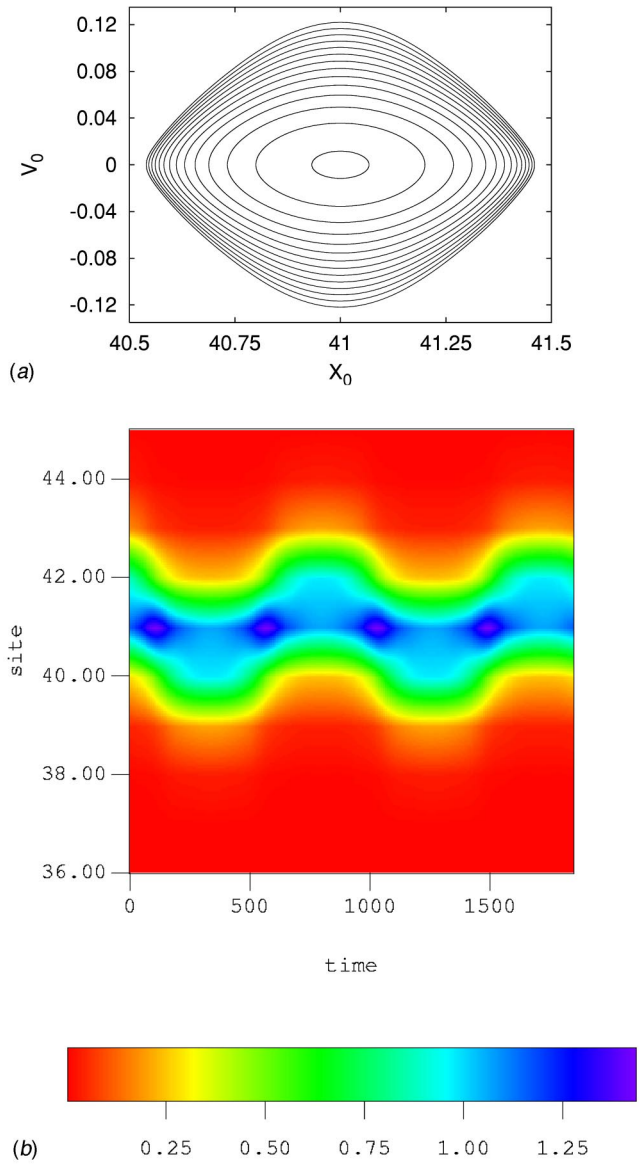

FIG. 17. (Color online). (a) Evolution of the localization center x_0 of an exact $(\frac{1}{18})$-oscillating breather for different values of ν: 0.05, 0.06,…, 0.18. The internal frequency is $\omega_b=3.086$. The amplitude of the oscillation of x_0 increases with ν, revealing the nonlinear character of the motion for the highest values of ν. (b) Density plot of the time evolution of $|\hat{\Phi}_n|^2$ for the above oscillating breather.

the existence of a background in the exact oscillating breather solutions and its behavior with the amplitude of the breather oscillations are fully consistent with the interpretation of the results obtained for the mobile solutions.

D. Validity and limitations of particle perspective

The most basic result of the perturbative collective variable theories away from the integrable regime is the existence of a Peierls–Nabarro potential function of the core (collective variable) center. It expresses (in particlelike terms) that the breather position is no longer indifferent because the continuous translational invariance has been broken. From this also naturally comes the existence of oscillating breathers. We have seen how our numerics fully confirm the qualitative validity of these predictions.

A further prediction concerns the phase portrait's transition studied in Ref. 35. Despite the fact that our end of continuation is correlated with the equipotential lines' profile of the numerical PN barriers, and the phase portrait transition is also related to their sudden growth, no clear connection (between transition and end of continuation) can be established. The end of continuation is itself sensibly interpreted as a numerical consequence of the sudden increases of the amplitude background, and does not imply neccesarily the existence of any global phase portrait transition.

However, in some respects the perturbative collective variable theory is clearly incomplete: For example, it is unable to predict the observed localized (core) instability bifurcation and the observed symmetry breaking transitions for $\nu<0$. These bifurcations could easily appear in a theory with (at least) two variables (a dimer) experiencing the Peierls–Nabarro potential, which would demand an improved perturbative ansatz. This improved ansatz must coincide in the integrable limit with the A-L solution. One can use the numerical results to guide the construction of such an improved ansatz. In this respect, the following observation may be relevant. The parameter β of the A-L solution determines both the amplitude and the width of the localized pulse. However, our numerical estimates of these breather characteristics for immobile breathers show clearly that, for fixed value of ω_b, the breather width is independent of ν, while the amplitude varies with it. In other words, away from integrability, width and amplitude of the (immobile) breather are no longer a single collective variable.

Beyond any other limitation of the perturbative collective variable theory, the background (an indispensable part of the exact solution) is absent in the perturbative ansatz, and it cannot appear later in that context. A complete theory of (nonlinear Schrödinger) breather motion should somehow incorporate the background in the ansatz itself. If correct, it should then predict that the background amplitude grows from zero with the nonintegrability parameter ν, and (ideally) so on with all the numerically observed behaviors. One possible way to develop the analytical approach could be to use the method presented in Ref. 41. In this scheme, Eq. (44) may play an important role, for it provides the energy balance governing the translational motion of the breather core. In other words, our results show that the core energy is not an invariant of motion and this requires the existence of a finely tuned background whose nonlinear interaction with the core compensates the core energy variations. We hope that the numerical work presented here will provide motivation for further analytical research.

V. CONCLUSIONS AND PROSPECTIVE REMARKS

We have studied numerically the problem of mobility of nonlinear localized solutions of the one-dimensional nonlinear Schrödinger lattice (7) using a regularized Newton method. This method allows us to continue the family of mobile Ablowitz–Ladik discrete breathers into the nonintegrable domain of model parameters. We find that these solu-

tions decay asymptotically, in space, to an excited lattice extended state (the background), whose amplitude vanishes at the integrable Ablowitz–Ladik limit. This component of the solution is unambiguously found to be a linear combination of nonlinear resonant plane waves whose amplitudes decay typically, in k-space, exponentially. The exponentially localized oscillation (the core) of the amplitude probability rides over this extended radiation state:

$$\hat{\Phi} = \hat{\Phi}_{core} + \hat{\Phi}_{backg}. \tag{48}$$

Numerically exact moving discrete breathers with an infinitely extended tail of small amplitude were already observed in some cases for Klein–Gordon lattices with Morse potential by Cretegny and Aubry,[20] however no investigation of the background of these exact solutions is reported, so they were able only to "…suggest that generally a strictly localized breather cannot propagate without radiating energy." Our systematic study of the NLS lattice allows us to go further by showing that the extended background (here fully characterized) plays an important and subtle role in the translational motion of the localized core. Indeed, it is an indispensable part of the exact solution in the nonintegrable regime. Exact mobile localization only exists over finely tuned extended states of the nonlinear lattice. Mobile "pure" (i.e., rest state background) localization must be regarded as very exceptional.[32]

The high numerical accuracy of the method allows a precise Floquet stability analysis of the moving discrete breather solutions. The Floquet analysis reveals the type of instabilities (both localized and extended) eventually experienced by the two-parameter family of moving breathers. Some generic bifurcations in the space of model parameters are thus identified. For negative values of the nonintegrability parameter ν, we find narrow regions where the immobile breathers experience mirror symmetry-breaking bifurcations and, simultaneously, the amplitude of the background component of the mobile breather solutions decreases down to almost negligible values.

The most relevant predictions of perturbative collective variable theory are confirmed by our numerical results, which show the existence of Peierls–Nabarro barriers to breather translational motion. Furthermore, the existence of exact oscillating breather solutions is numerically confirmed. They are found to contain an extended background whose amplitude is typically much smaller than for mobile breathers.

The Peierls–Nabarro barrier E_{PN}, computed from immobile breathers, and the amplitude background of moving breathers are found to be strongly correlated, which correctly suggests that the background has a role in the energy balance required to overcome the barriers to translational motion. This is also fully consistent with the observations on the background amplitude behavior of spatially oscillating anchored breathers. Indeed, assuming the simplest case of a monochromatic background, the variation of the core energy during its translational motion is exactly compensated by the variation of the energy of interaction between the localized core and the background. Currently used effective particle (collective variable) theories are thus seen as intrinsically incomplete, because core energy is not an invariant of motion. Any sensible improved approach must adopt Eq. (48) as a starting point for improved perturbative ansatze, and we hope that our work will stimulate further studies along these lines.

There are, at very different levels, several open questions to further research. From a technical point of view, it is important to analyze carefully the irrational limit $p/q \to \sigma$ of the solutions. In particular, in this limit the number of resonant plane wave branches tends to a continuum and one could (or not) expect that exponential localization in the reciprocal lattice persists in that limit. This can be addressed numerically, though systematic investigations may require some efforts in optimizing the time efficiency of current numerical schemes.

An important issue regarding applications is the phenomenology of multibreather states. In particular, studies on collisions of a pair of breathers may find in this study of exact mobility a useful reference in order to deal with the complexities that emerge from the many time-length scales involved in these physically relevant phenomena. Much simpler multibreather states, e.g., trainlike chains of (moderately) separated moving breathers, could also be investigated. At least, the perspective and results presented here may be of some interest to studies of the effects of coupling to (nonthermal and/or thermal) radiation baths in the breather and multibreather states of nonlinear lattices[42] and the practical manipulation and patterning of localized "hot spots" by external fields.[43]

ACKNOWLEDGMENTS

We acknowledge interesting discussions with P. Kevrekidis, B. Malomed, S. Flach, F. Falo, J. L. García-Palacios, P. J. Martínez, J.-A. Sepulchre, and G. P. Tsironis. We are grateful to the organizers of the workshop "*Intrinsic localized modes and discrete breathers in nonlinear lattices*" at Erice, where this collaboration was initiated. Financial support came from LOCNET HPRN-CT-1999-00163, MCyT (Project No. BFM2002–00113), DGA and BIFI. J.G.-G. acknowledges financial support of the MECyD through a FPU grant. Work at Los Alamos performed under the auspices of the US DoE. J. G.-G. would like to dedicate his contribution to this work to the memory of his grandfather who recently disappeared.

[1] A. C. Scott, *Nonlinear Science: Emergence and Dynamics of Coherent Structures* (Oxford University Press, Oxford, 1999).
[2] M. Peyrard, Nonlinearity **17**, R1 (2004).
[3] S. F Mingaleev, Yu. B. Gaididei, P. L. Christiansen, and Yu. S. Kivshar, Europhys. Lett. **59**, 403 (2002).
[4] A. McGurn, Chaos **13**, 754 (2003).
[5] Y. S. Kivshar and G. P. Agrawal, *Optical Solitons: From Fibers to Photonic Crystals* (Academic, San Diego, 2003).
[6] J. W. Fleischer, M. Segev, N. K. Efremidis, and D. N. Christodoulides, Nature (London) **422**, 147 (2003); D. N. Christodoulides and R. I. Joseph, Opt. Lett. **13**, 794 (1988); H. S. Eisenberg and Y. Silbergerg, Phys. Rev. Lett. **81**, 3383 (1998); R. Morandotti, U. Peschel, J. S. Aitchison, H. S. Eisenberg, and Y. Silberberg, *ibid.* **83**, 2726 (1999); **83**, 4756 (1999); **86**, 3296 (2001).
[7] A. J. Leggett, Rev. Mod. Phys. **73**, 307 (2001).
[8] E. Trías, J. J. Mazo, and T. P. Orlando, Phys. Rev. Lett. **84**, 741 (2000).
[9] P. Binder, D. Abraimov, A. V. Ustinov, S. Flach, and Y. Zolotaryuk, Phys.

Rev. Lett. **84**, 745 (2000).
[10]K. E. Strecker, G. B. Patridge, A. G. Truscott, and R. G. Hulet, Nature (London) **417**, 150 (2002); F. Dalfovo, S. Giorgini, L. P. Pitaevskii, and S. Stringari, Rev. Mod. Phys. **71**, 463 (1999); J. Denschlag, J. E. Simsarian, D L. Feder, Ch. W. Clark, L. A. Collins, J. Cubizolles, L. Deng, E. W. Hagley, K. Helmerson, W. P. Reinhardt, S. L. Rolston, B. I. Schneider, and W. D. Phillips, Science **287**, 97 (2000).
[11]F. S. Cataliotti, S. Burger, C. Fort, P. Maddaloni, F. Minardi, A. Trombettoni, A. Smerzi, and M. Inguscio, Science **293**, 843 (2001); A. Smerzi, A. Trombettoni, P. G. Kevrekidis, and A. R. Bishop, Phys. Rev. Lett. **89**, 170402 (2002).
[12]A. Smerzi, S. Fantoni, S. Giovanazzi, and S. R. Shenoy, Phys. Rev. Lett. **79**, 4950 (1997); A. Trombettoni and A. Smerzi, *ibid.* **86**, 2353 (2001).
[13]D. K. Campbell, S. Flach, and Yu. S. Kivshar, Phys. Today **57** (1), 43 (2004).
[14]Y. Kivshar and S. Flach, Chaos **13**, 586 (2003).
[15]J. L. Marín, F. Falo, P. J. Martínez, and L. M. Floría, Phys. Rev. E **63**, 066603 (2001); P. J. Martínez, L. M. Floría, A. Meister, and F. Falo, Chaos **13**, 610 (2003); D. Zueco, F. Falo, P. J. Martínez, and L. M. Floría (unpublished).
[16]M. Salerno, Phys. Rev. A **46**, 6856 (1992).
[17]J. Gómez-Gardeñes, F. Falo, and L. M. Floría, Phys. Lett. A **332**, 213 (2004).
[18]J. C. Eilbeck and M. Johansson, in *Proceedings of "Localization and Energy Transfer in Nonlinear Systems,"* edited by L. Vázquez, R. S. MacKay, and M. P. Zorzano (World Scientific, Singapore, 2003), p. 44.
[19]M. J. Ablowitz and J. F. Ladik, Stud. Appl. Math. **55**, 213 (1976); J. Math. Phys. **17**, 1011 (1976).
[20]S. Aubry and T. Cretegny, Physica D **119**, 34 (1998).
[21]S. Flach and K. Kladko, Physica D **127**, 61 (1999).
[22]T. Cretegny and S. Aubry, Phys. Rev. B **55**, R11929 (1997).
[23]J. L. Marín and S. Aubry, Nonlinearity **9**, 1501 (1996).
[24]R. S. Mackay and S. Aubry, Nonlinearity **7**, 1623 (1994).
[25]G. Strang, *Linear Algebra*, 2nd ed. (Academic, New York, 1980).
[26]W. H. Press, S. A. Teukolsky, W. T. Vetterling, and B. P. Flannery, *Numerical Recipes* (Cambridge University Press, New York, 1992).
[27]J. L. Marín, S. Aubry, and L. M. Floría, Physica D **113**, 283 (1998).
[28]Y. S. Kivshar and M. Peyrard, Phys. Rev. A **46**, 3198 (1992).
[29]Y. S. Kivshar and M. Salerno, Phys. Rev. E **49**, 3543 (1994).
[30]S. V. Dmitriev, P. G. Kevrekidis, B. A. Malomed, and D. J. Frantzeskakis, Phys. Rev. E **68**, 056603 (2003).
[31]D. B. Duncan, J. C. Eilbeck, H. Feddersen, and J. A. D. Wattis, Physica D **68**, 1 (1993).
[32]S. Flach, Y. Zolotaryuk, and K. Kladko, Phys. Rev. E **59**, 6105 (1999).
[33]J. L. Marín and S. Aubry, Physica D **119**, 163 (1998).
[34]A. A. Vakhnenko and Y. B. Gaididei, Teor. Mat. Fiz. **68**, 350 (1986) [Theor. Math. Phys. **68**, 873 (1987)].
[35]C. Claude, Yu. S. Kivshar, O. Kluth, and K. H. Spatschek, Phys. Rev. B **47**, 14 228 (1993).
[36]D. Cai, A. R. Bishop, and N. Gronbech-Jensen, Phys. Rev. Lett. **72**, 591 (1994); Phys. Rev. E **53**, 4131 (1996).
[37]K. Kundu, Phys. Rev. E **61**, 5839 (2000).
[38]R. S. Mackay and J.-A. Sepulchre, J. Phys. A **35**, 3985 (2002); J-A. Sepulchre, in *Proceedings of "Localization and Energy Transfer in Nonlinear Systems,"* edited by L. Vázquez, R. S. McKay, and M. P. Zorzano (World Scientific, Singapore, 2003), p. 102; R. S. Mackay, in *Energy Localisation and Transfer*, edited by T. Dauxois A. Litvak-Hinenzon, R. S. MacKay, and A. Spanoudaki (World Scientific, Singapore, 2004), p. 149.
[39]Y. S. Kivshar and D. K. Campbell, Phys. Rev. E **48**, 3077 (1993).
[40]However, in Ref. 32 the authors find particular on-site potentials for Klein–Gordon lattices for which moving kinks and pulses do not possess an infinite tail, though immobile breathers do experience a Peierls–Nabarro barrier.
[41]R. Boesch and M. Peyrard, Phys. Rev. B **43**, 8491 (1991).
[42]K. O. Rasmussen, S. Aubry, A. R. Bishop, and G. P. Tsironis, Eur. Phys. J. B **15**, 169 (2000).
[43]D. Cai, A. R. Bishop, N. Gronbech-Jensen, and M. Salerno, Phys. Rev. Lett. **74**, 1186 (1995).